

7/7/2023 9:14:18 AM

# Compare Results

Old File:

**MallardStasis.pdf**

**58 pages (2.64 MB)**

7/3/2023 6:18:14 PM

versus

New File:

**manuscript.pdf**

**63 pages (2.84 MB)**

7/7/2023 7:07:58 AM

**Total Changes**

**1163**

**Content**

**416** Replacements

**290** Insertions

**232** Deletions

**Styling and Annotations**

**108** Styling

**117** Annotations

[Go to First Change \(page 2\)](#)

# Phenotypic stasis with genetic divergence

François Mallard<sup>1,\*</sup>

Luke Noble<sup>1</sup>

Thiago Guzella<sup>1</sup>

Bruno Afonso<sup>1</sup>

Charles F. Baer<sup>2</sup>

Henrique Teotónio<sup>1,\*</sup>



1. Institut de Biologie de l'École Normale Supérieure, CNRS UMR 8197, Inserm U1024, PSL Research University, F-75005 Paris, France;

2. Department of Biology, University of Florida Genetics Institute, University of Florida, Gainesville, Florida 32611, U.S.A.;

\* Corresponding authors: mallard@bio.ens.psl.eu, teotonio@bio.ens.psl.eu.

**Keywords:** phenotypic stasis, G-matrix, selection surface, genetic drift, locomotion behavior, transition rates, *Caenorhabditis elegans*, experimental evolution.

# 1 Abstract

1  
2 Whether or not genetic divergence on the short-term of tens to hundreds of generations is com-  
3 patible with phenotypic stasis remains a relatively unexplored problem. We evolved predomi-  
4 nantly outcrossing, genetically diverse populations of the nematode *Caenorhabditis elegans* under  
5 a constant and homogeneous environment for 240 generations, and followed individual locomo-  
6 tion behavior. **Although** founders of lab populations show highly diverse locomotion behavior,  
7 during lab evolution the component traits of locomotion behavior – defined as the transition rates  
8 in activity and direction – did not show divergence from the ancestral population. In contrast,  
9 **transition rates'** genetic (co)variance structure **showed a** marked divergence from the ancestral  
10 state and differentiation among replicate populations during the final 100 generations and after  
11 most adaptation had been achieved. We observe that genetic differentiation is a transient pattern  
12 during the loss of genetic variance along phenotypic dimensions under drift during the last 100  
13 generations of lab evolution.  These results suggest that once adaptation has occurred, and on the  
14 short-term of tens of generations, stasis of locomotion **behavior is maintained** because of effec-  
15 tive stabilizing selection at a large phenotypic **scale. At the same time,** the genetic structuring of  
16 component traits is contingent upon drift history at a local phenotypic scale. 




## 2 Introduction



17  
18 Stasis, the lack of directional change in the average values of a trait over time, is the most common  
19 phenotypic pattern observed over timespans reaching one million years (Arnold, 2014; Gingerich,  
20 2019; Uyeda et al., 2011). Theory predicts phenotypic stasis when stabilizing selection, or when  
21 directional and other forms of selection cancel out over the period examined, acts upon standing  
22 genetic variation reflecting the phenotypic effects of mutational input (Charlesworth et al., 1982;  
23 Estes and Arnold, 2007; Hansen and Martins, 1996; Lande, 1986; Morrissey and Hadfield, 2012).  
24 When considering mutation-selection balance on the long-term (as scaled by the effective popula-  
25 tion sizes), theory has been successfully applied to explain, for example, fly wing evolution over  
26 a period of 40 million years (Houle et al., 2017), or nematode embryogenesis over 100 million  
27 years (Farhadifar et al., 2015). On the short-term of a few tens to hundreds of generations, how-  
28 ever, many natural populations depend on standing genetic variation for adaptation or rescue  
29 from extinction, when mutation should be of little influence and founder effects, demographic  
30 stochasticity and genetic drift are important (Chelo et al., 2013; Hill, 1982; Mallard et al., 2022b;  
31 Matuszewski et al., 2015).

32 On the short-term, before mutation-selection balance is reached, phenotypic stasis in natural  
33 populations is also commonly observed, often despite significant trait heritability and selection  
34 (Merilä et al., 2001; Pujol et al., 2018). Explanations for short-term phenotypic stasis have re-  
35 lied on showing that in many cases there were no changes in the breeding traits' values, that  
36 is, no genetic divergence, either because of selection on unmeasured traits that are genetically  
37 correlated with observed ones or because of correlated selection due to unknown environmen-  
38 tal covariation between observed and unobserved traits with fitness e.g., (Czorlich et al., 2022;  
39 Kruuk et al., 2002), both instances of "indirect" selection. Short-term phenotypic stasis with-  
40 out genetic divergence has also been explained by phenotypic plasticity allowing the tracking  
41 of environmental fluctuations e.g., (Biquet et al., 2022; de Villemereuil et al., 2020). Pujol et al.  
42 (2018) reviews other processes responsible for phenotypic stasis in the short term. These studies

43 indicate that phenotypic evolution cannot be understood when considering each trait indepen-  
44 dently of others and that a multivariate description of selection and standing genetic variation is  
45 needed. Selection on multiple traits should be seen as a surface with potentially several orthog-  
46 onal dimensions (Phillips and Arnold, 1989), each with particular gradients depicting selection  
47 strength and direction on each trait and between traits (Arnold et al., 2001; Lande and Arnold,  
48 1983). Responses to selection in turn will depend on the size and shape of the **G-matrix**, the addi-  
49 tive genetic variance-covariance matrix of multiple traits (Lande, 1979). For example, phenotypic  
50 dimensions with more genetic variation are expected to facilitate adaptation, as selection will be  
51 more efficient (Lande, 1976, 1979; Schluter, 1996), even if indirect selection can confound predic-  
52 tions about phenotypic evolution (Mallard et al., 2022a; Morrissey and Bonnet, 2019; Stinchcombe  
53 et al., 2014).

54 The extent to which phenotypic stasis is compatible with the expected divergence of the  
55 **G-matrix** in the short-term remains little unexplored cf. (Bohren et al., 1966; Gromko, 1995;  
56 Simões et al., 2019; Teotónio et al., 2004; Teotónio and Rose, 2000). Studies in natural populations  
57 cannot usually control environmental variation and estimates of **G-matrix** dynamics are nearly  
58 impossible to obtain, while experiments employing truncation selection do not easily model  
59 the complexity of the selection surface. Under drift, and assuming an infinitesimal model of  
60 trait inheritance, the **G-matrix** size (i.e., the total genetic variance) is reduced and diverges from  
61 ancestral states by a factor proportional to the effective population size (Lande, 1976; Lynch and  
62 Hill, 1986; Phillips et al., 2001). However, theory that includes the effects of finite population  
63 sizes, multivariate selection, and the pleiotropic effects of mutation remains out of reach for  
64 changes in genetic covariances between traits and thus **G-matrix** shape (Barton and Turelli, 1987;  
65 Burger, 2000; Lande, 1980; Lynch and Walsh, 1998; Simons et al., 2018). We do expect, however,  
66 that once most adaptation has occurred, the divergence of the **G-matrix** shape is caused by  
67 drift, and also know that different forms of selection might lead to further genetic divergence in  
68 the relatively local phenotypic space occupied after adaptation (Doroszuk et al., 2008; Haller and  
69 Hendry, 2014). Whether or not genetic divergence will also lead to phenotypic divergence should

70 then depend on the distribution of pleiotropic effects of quantitative trait loci (QTL) alleles, and  
71  linkage disequilibrium between them, created by past selection and drift, and ultimately on the  
72 developmental and physiological mapping of genetic onto phenotypic variation (Chebib and  
73 Guillaume, 2017; Hansen and Wagner, 2001; Morrissey, 2015; Riska, 1989).

74 Here we seek to find if the short-term evolution of the **G-matrix** follows the directions of  
75 selection or if there is loss of genetic variance just by drift. We also seek to determine how ge-  
76 netic divergence is compatible with phenotypic stasis once most adaptation has been achieved.  
77 We analyze the evolution of locomotion behavior on the hermaphroditic nematode *Caenorhabditis*  
78 *elegans*, spanning 240 generations of lab evolution in a constant and homogeneous environment,  
79 thus maximizing the chances of imposing and detecting stabilizing selection. We could obtain  
80 an accurate characterization of the fitness effects of component trait variation of locomotion be-  
81 havior (transition rates between movement states and direction), by measuring essentially all  
82 individuals at the time of reproduction. We expect locomotion behavior to evolve because indi-  
83 vidual nematodes do not need to engage in foraging for feeding themselves (Gray et al., 2005).  
84 It is further expected that sexual interaction between hermaphrodites and males will further im-  
85 pact the evolution of locomotion behavior (Barr et al., 2018). We characterized the evolution of  
86 the broad-sense **G-matrix** for hermaphrodite locomotion behavior, obtained by phenotyping in-  
87 bred lines derived from the domesticated ancestral population at generation 140, and from three  
88  replicate populations during further 50 and 100 generations in the same environment. After  
89 domestication, selection gradients were estimated by regressing fertility onto transition rates. 

## 90 **3 Methods**

### 91 **3.1 Archiving**

92 Data, R code scripts, and modeling results (including **G-matrix** estimates) can be found in our  
93 [github repository](#).

## 3.2 Laboratory culture

94  
95 We analyzed the lab evolution of locomotion behavior during 273 generations (Figure 1A), the  
96 first 223 of which have been previously detailed (Noble et al., 2017; Teotónio et al., 2012; The-  
97 ologidis et al., 2014). Briefly, 16 inbred founders were intercrossed in a 33-generation funnel  
98 to obtain a single hybrid population (named A0), from which six population replicates (A[1-6])  
99 were domesticated for 140 generations. Based on the evolution of several life-history traits such  
100 as hermaphrodite self and outcross fertility, male mating ability or viability until reproduction we  
101 have previously shown that most adaptation to lab conditions had occurred by generation 100  
102 (Carvalho et al., 2014a,b; Pouillet et al., 2016; Teotónio et al., 2012; Theologidis et al., 2014). From  
103 population A6 at generation 140 (A6140), we derived six replicate populations and maintained  
104 them in the same environment for another 100 generations (CA[1-6]). CA[1-6] were derived  
105 from splitting into six a single pool of at least  $10^3$  individuals from large ( $10^4$ ) thawed sam-  
106 ples of the A6140 population (Theologidis et al., 2014). Inbred lines were generated by selfing  
107 hermaphrodites from A6140 (for at least 10 generations), and from CA populations 1-3 at gener-  
108 ation 50 and 100 (CA[1-3]50 and CA[1-3]100; Noble et al. (2019)). We refer to these last 100  
109 generations as the focal stage. During the domestication and focal stages, populations were cul-  
110 tured at constant census sizes of  $N = 10^4$  and expected effective population sizes of  $N_e = 10^3$   
111 (Chelo et al., 2013; Chelo and Teotónio, 2013). Non-overlapping 4-day life-cycles were defined  
112 by extracting embryos from plates and seeding starvation-synchronized L1 larvae to fresh food  
113 (Teotónio et al., 2012). Periodic storage of samples ( $> 10^3$  individuals) was done by freezing  
114 (Stiernagle, 1999). Revival of ancestral and derived population samples allows us to control for  
115 transgenerational environmental effects under "common garden" phenotypic assays (Teotónio  
116 et al., 2017).

117

### 3.3 Worm tracking assays

#### 118 3.3.1 Sampling and design



119 Population samples were thawed from frozen stocks on 9cm Petri dishes and grown until ex-  
120 haustion of food (*Escherichia coli* HT115). This occurred 2-3 generations after thawing, after which  
121 individuals were washed from plates in M9 buffer. Adults were removed by centrifugation, and  
122 three plates per line were seeded with around 1000 larvae. Samples were maintained for one to  
123 two complete generations in the controlled environment of lab evolution. At the assay generation  
124 (generation 4-6 generations post-thaw), adults were phenotyped for locomotion behavior at their  
125 usual reproduction time during lab evolution (72h post L1 stage seeding) in single 9 cm plates.  
126 At the beginning of each assay we measured ambient temperature and humidity in the imaging  
127 room to control for their effects on locomotion.


128 Inbred lines from the experimental populations were phenotyped over three main common  
129 garden experiments in two different lab locations (Lisbon and Paris) by three experimenters.  
130 The first common garden included only A6140 lineages, the second CA[1-3]50 lineages and the  
131 last one all CA[1-3]100 lineages and A6140 lineages. A6140 G-matrix was initially estimated only  
132 from the first common garden (see details below). There were 197 independent thaws, each defin-  
133 ing a statistical block containing 2-22 samples. 188 inbred lines from the A6140 population were  
134 phenotyped, with 52 CA150, 52 CA250, 51 CA350, 51 CA1100, 53 CA2100 and 68 from CA3100  
135 (not including the A6140 lineages from the third common garden). Each line was phenotyped  
136 in at least two blocks (technical replicates). CA[1-3]50 and CA[1-3]100 lines were phenotyped  
137 within a year. A6140 lines were phenotyped over two consecutive years. A set of 63 A6140  
138 lineages that were phenotyped together with the CA[1-3]100 populations in the third common  
139 garden were used to compute a second A6140 G-matrix. We further phenotyped the outbred  
140 populations and the 16 founders in a single common garden. For these, there were 9 indepen-  
141 dent thaws, of which 5 also contained founders. All founders and populations were phenotyped  
142 twice except for A6140, which was included in six blocks.



143 To improve the estimation of the selection surface in our lab evolution environment (see  
144 below), we also assayed locomotion bias in 56 inbred lines derived from populations evolved in  
145 a high-salt environment (GA[1,2,4]50) for which fertility data was available (Noble et al., 2017).  
146 These lines were phenotyped in the same blocks as the A6140 lines included in the gamma matrix  
147 analysis (first common garden, single experimenter). Removing these lines from the analysis did  
148 not affect the mode of the posterior distribution estimates of our coefficients. It only led to the  
149 loss of statistical power reflected by wider credible intervals (analysis not shown).

### 150 3.3.2 *Imaging*

151 To measure locomotion behavior we imaged adults 72h post-L1 seeding using the Multi-Worm  
152 Tracker [MWT version 1.3.0; Swierczek et al. (2011)]. Movies were obtained with a Dalsa Fal-  
153 con 4M30 CCD camera and National Instruments PCIe-1427 CameraLink card, imaging through  
154 a 0.13-0.16 mm cover glass placed in the plate lid, illuminated by a Schott A08926 backlight.  
155 Plates were imaged for approximately 20-25 minutes with default MWT acquisition parameters.  
156   Choreography was used to filter and extract the number and persistence of tracked objects and  
157 assign movement states across consecutive frames as forward, still or backwards, assuming that  
158 the dominant direction of movement in each track is forward (Swierczek et al., 2011).

159 MWT detects and loses objects over time as individual worms enter and leave the field of  
160 view or collide with each other. Each  track is a period of continuous observation for a single  
161 object (the mapping between individual worms and tracks is not 1:1). We ignored the first 5  
162 minutes of recording, as worms are perturbed by plate handling. Each movie contains around  
163 1000 tracks with a mean duration of about 1 minute. The MWT directly exports measurements at  
164 a frequency that can vary over time (depending on tracked object density and computer resource  
165 availability), so data were standardized by subsampling to a common frame rate of 4 Hz. Worm  
166 density, taken as the mean number of tracks recorded at each time point averaged over the total  
167 movie duration, was used as a covariate in the estimation of genetic variance-covariances below.

### 168 3.3.3 Differentiating males from hermaphrodites

169 A6140 and all CA populations are androdioecious, with hermaphrodites and males segregating  
170 at intermediate frequencies (Teotónio et al., 2012; Theologidis et al., 2014). We were able to  
171 reliably (97% accuracy) differentiate between the sexes based on behavioral and morphological  
172 traits extracted from MWT data.

173 We first evaluated a set of simple descriptions of individual size, shape, and movement to  
174 find a subset of metrics that maximized the difference in preference for a two-component model  
175 between negative and positive controls: respectively, inbred founders and two monoecious (M)  
176 populations which contained no, or very few, males; and three dioecious (D) populations with  
177 approximately 50% males [M and D populations were derived from A6140, see Theologidis  
178 et al. (2014) and Guzella et al. (2018)]. Starting with worm area, length, width, curvature, ve-  
179 locity, acceleration, and movement run length as parent traits from the Choreography output,  
180 derived descendant traits were defined by first splitting parents by individual movement state  
181 (forward, backward, still) and calculating the median and variance of the distribution for each  
182 track. Traits with more than 1% missing data were excluded, and values were log-transformed  
183 where strongly non-normal (a difference in Shapiro-Wilk  $-\log_{10}(p) > 10$ ). Fixed block and  
184 log plate density effects were removed by linear regression before fitting the residuals to two-  
185 component Gaussian mixture models. These two-component Gaussian models were fit to tracks  
186 for each line/population [R package *mclust* Scrucca et al. (2016), VII spherical model with vary-  
187 ing volume], orienting labels by area (assuming males are smaller than hermaphrodites). We  
188 sampled over sets of three traits, requiring three different parent trait classes, at least one related  
189 to size. We took the set maximizing the difference in median Integrated Complete-data Likeli-  
190 hood (ICL) between control groups (log area, log width, and velocity, all in the forward state).  
191 By this ranking, the 16 inbred founders and two monoecious populations fell within the lower  
192 19 samples (of 77), while the three dioecious populations fell within the top 15 samples.

193 To build a more sensitive classifier robust to male variation beyond the range seen in control

194 data, we then trained an extreme gradient boosting model using the full set of 30 derived traits on  
 195 the top/bottom 20 samples ranked by ICL in the three-trait mixture model [R package *xgboost*,  
 196 [Chen and Guestrin \(2016\)](#)]. Negative control samples were assumed to be 100% hermaphrodite,  
 197 while tracks in positive controls were assigned based on *mclust* model prediction, excluding  
 198 those with classification uncertainty in the top decile. Tracks were classified by logistic regression,  
 199 weighting samples inversely by size, with the best cross-validated model achieving an area under  
 200 the precision-recall curve of 99.75% and a test classification error of 3.1% ( $max\_depth = 4, eta =$   
 201  $0.3, subsample = 0.8, eval\_metric = "error"$ ). Prediction probabilities were discretized at 0.5.

202 Males tend to move much faster than hermaphrodites ([Lipton et al., 2004](#)), and because in-  
 203 dividual collision leads to loss of tracking, sex is strongly confounded with track length and  
 204 number. To estimate male frequencies at the sample level, tracks were sampled at 1s slices every  
 205 30s over each movie in the interval 400-1200 seconds, and line/population estimates were ob-  
 206 tained from a binomial generalized linear model ([Venables and Ripley, 2002](#)). Estimates appear  
 207 to saturate at around 45%, presumably due to density-dependent aggregation of multiple males  
 208 attempting to copulate.

### 209 3.4 Locomotion behavior

#### 210 3.4.1 Definition of transition rates

211 In a one-dimensional space, individual locomotion behavior can be described by the transition  
 212 rates of activity and direction. We modeled the expected sex-specific transition rates between for-  
 213 ward, still and backward movement states with a continuous time Markov process. We consider  
 214 a system having  $d = 3$  states with  $P(t_1, t_2) \in \mathbb{R}^{d,d}$ ,  $t_2 > t_1$ , denoting the transition probability  
 215 matrix ([Jackson, 2011](#); [Kalbfleisch and Lawless, 1985](#)):

$$p_{i,j}(t_1, t_2) = \mathbb{P}[s(t_2) = j \mid s(t_1) = i] \quad (1)$$

216 where  $s(t) \in \mathcal{S}$ , with  $\mathcal{S} = \{\underline{s}till, \underline{f}orward, \underline{b}ackward\}$  being the movement state occupied in instant  
 217  $t$ . We consider a time-homogeneous process described by the transition rate matrix:

$$Q \equiv \begin{bmatrix} -q_s & q_{s,f} & q_{s,b} \\ q_{f,s} & -q_f & q_{f,b} \\ q_{b,s} & q_{b,f} & -q_b \end{bmatrix} \quad (2)$$

218 where  $q_{i,j} \geq 0 \forall i, j$ , subject to the constraint:

$$q_i = \sum_{j \neq i} q_{i,j} \quad (3)$$

219 Hence, six of the nine possible transitions are independent. Let  $\theta$  denote the parameters to be  
 220 estimated, containing the off-diagonal elements from equation 2:

$$\theta = [q_{s,f}, q_{s,b}, q_{f,s}, q_{f,b}, q_{b,s}, q_{b,f}] \quad (4)$$

221 In this model, **an object's time** remains in a given state is on average  $1/q_i$ . Since the process  
 222 is stationary, the probability of transition is a function of the time difference  $\Delta t = t_2 - t_1$ , such  
 223 that  $P(t_1, t_2) = P(\Delta t)$ , and the elements of the  $P(\Delta t)$  matrix:

$$p_{i,j}(\Delta t) = \mathbb{P} [S(\Delta t) = j \mid S(0) = i] \quad (5)$$

224 It then follows that:

$$P(\Delta t) = \exp(\Delta t Q) \quad (6)$$

225 where  $\exp(\cdot)$  denotes the matrix exponential. The constraint in equation 3 ensures that:

$$P(\infty) = \begin{bmatrix} f_s & f_f & f_b \\ f_s & f_f & f_b \\ f_s & f_f & f_b \end{bmatrix} \quad (7)$$

226 where  $f_i$  is the relative frequency of state  $i$  that no longer depends on the previous state (all  
 227 three rows of the  $P(\infty)$  matrix converge). We find that the state frequencies from  $P(\infty)$  are a  
 228 monotonic and mostly linear function of the observed frequencies of movement states (Figure S3),  
 229 showing that violations of the Markov assumption of the model do not induce a large bias in the  
 230 long-term predictions of our model.

### 231 3.4.2 Estimation of transition rates

232 To estimate transition rates, we have  $N$  objects (individual tracks) from each technical replicate  
 233 (Petri plate), with the data on the  $k$ -th object denoted as:

$$\mathcal{D}_k = (x_{k,1}, x_{k,2}, \dots, x_{k,n_k-1}) \quad (8)$$

$$x_{k,l} = (s_{k,l}, s_{k,l+1}, \Delta t_{k,l}), \Delta t_{k,l} = t_{k,l+1} - t_{k,l} > 0 \quad (9)$$

234 where  $s_{k,l}$  is the state of the  $k$ -th object in the  $l$ -th time-point in which it was observed,  
 235 and  $t_{k,l}$  is the instant of time in which this observation was made. Then, given data  $\mathcal{D} =$   
 236  $\{\mathcal{D}_1, \mathcal{D}_2, \dots, \mathcal{D}_N\}$ , the log-likelihood for the model for analysis is (Bladt and Sorensen, 2005;  
 237 Kalbfleisch and Lawless, 1985):

$$\mathcal{L}(\theta | \mathcal{D}) = \sum_{k=1}^N \sum_{l=1}^{n_k-1} \ln(p_{i,j}(\Delta t) |_{i=s_{k,l}, j=s_{k,l+1}, \Delta t=\Delta t_{k,l}}) \quad (10)$$

238 where  $p_{i,j}(\Delta t)$  was defined in equation 5, and is calculated as a function of the parameters  
 239  $\theta$  via equation 4. Therefore, the data on the  $N$  objects can be represented as the number of  
 240 observations of  $x = (i, j, \Delta t)$ , which we denote as  $\tilde{n}_{i,j,\Delta t}$ :

$$\tilde{n}_{i,j,\Delta t} = \sum_{k=1}^N \sum_{l=1}^{n_k-1} \mathbb{I}_{i,j,\Delta t} [s_{k,l}, s_{k,l+1}, \Delta t_{k,l}] \quad (11)$$

241 and where  $\mathbb{I}_{i,j,\Delta t} [\cdot]$  is the indicator function:

$$\mathbb{I}_{i,j,\Delta t} [s_1, s_2, \delta t] = \begin{cases} 1, & \text{if } s_1 = i, s_2 = j \text{ and } \delta t = \Delta t \\ 0, & \text{otherwise} \end{cases} \quad (12)$$

242 The input data can then be compressed by considering only the data:

$$\mathcal{Z} = \{z_1, z_2, \dots, z_M\} \quad (13)$$

$$z_k = (\Delta t_k, \tilde{N}_k), \Delta t_k \in \mathfrak{R}^+, \tilde{N}_k \in \mathbb{N}_0^{d,d} \quad (14)$$

$$\tilde{N}_k = \tilde{n}_{i,j,\Delta t_k} \quad (15)$$

243 The log-likelihood to estimate transition rates can be finally rewritten as:

$$\mathcal{L}(\theta | \mathcal{Z}) = \sum_{k=1}^m \vec{\mathbb{1}}_d^T \left( \tilde{N}_k \odot \ln(P_k) \right) \vec{\mathbb{1}}_d \quad (16)$$

244 where  $\vec{\mathbb{1}}_d$  is a  $d$ -dimensional vector of 1s,  $\odot$  denotes the Hadamard product, and  $\ln P_k$  is the  
 245 matrix obtained by taking the logarithm of each value in matrix  $P_k$ .

246 These models were specified using RStan ([Stan Development Team \(2018\)](#), R version 3.3.2,  
 247 RStan version 2.15.1), which performs Bayesian inference using a Hamiltonian Monte Carlo sam-  
 248 pling to calculate the posterior probability of the parameters given the observed data. We used

249 multi-log normal prior distributions with mean transition rate and a coefficient of variation:

$$250 \ln(q_{i,j}) \sim \mathcal{N}(\ln(2), 0.6).$$

251 Throughout, we denote non-self transition rates  $q_k$  the six off-diagonal elements of the  $\mathbf{Q}$   
252 matrix estimated by the above model.

### 253 3.4.3 Male and inbreeding effects

254 Using the transition rates measured in populations and inbred lines, we fit a series of linear  
255 mixed-effects models to test for phenotypic evolution in the outbred **populations**, for effects of  
256 male frequency on hermaphrodite transition rates in the outbred **populations**, and for inbreeding  
257 effects in the inbred **lines**. Given sparse temporal sampling, we make the conservative assump-  
258 tion of independence of observations within domestication and focal stages. For transition rate  
259  $q_k$ :

$$\ln(q_k) = \alpha + \beta_{gen}G + \gamma_{anc}t + \delta_{anc} + \zeta_b + \epsilon \quad (17)$$

260 with  $\alpha$  the trait mean,  $\beta_{gen}$  a fixed effect of generation number  $t$ ,  $\gamma_{anc}$  and  $\delta_{anc}$  random effects  
261 accounting for intercept and slope differences between the domestication and focal periods of  
262 lab evolution (both  $\sim \mathcal{N}(0, \sigma^2)$ ),  $\zeta \sim \mathcal{N}(0, \sigma^2)$  a random effect of block  $b$  and  $\epsilon \sim \mathcal{N}(0, \sigma^2)$  the  
263 residual error.

$$\ln(q_k) = \alpha + \beta F + \gamma_{popId} + \zeta_b + \epsilon \quad (18)$$

264 with  $\beta$  a fixed effect of male frequency  $F$ ,  $\gamma_{popId} \sim \mathcal{N}(0, \sigma^2)$  a random effect accounting for  
265 differences between populations,  $\zeta \sim \mathcal{N}(0, \sigma^2)$  a random effect of block  $b$ , and  $\epsilon \sim \mathcal{N}(0, \sigma^2)$  the  
266 residual error.

267 As we estimate the  $\mathbf{G}$ -matrix from the line differences (see next section), it is likely that it  
268 does not reflect the true additive genetic (co)variance matrix ( $\mathbf{G}$ -matrix) unless the mean trait

269 values among lines are similar to the mean trait values of the outbred population from which the  
270 lines were derived (Lynch and Walsh, 1998). Only with directional, genome-wide, dominance  
271 or epistasis would the "broad-sense" **G**-matrix not be a good surrogate for the "narrow-sense"  
272 additive **G**-matrix. See Chapter 3 of Kearsey and Pooni (1996) for the different ways dominance  
273 and epistasis can change segregation variance in F2 crossing designs. Because the lines and the  
274 populations were phenotyped at different times, we included environmental covariates:

$$\ln(q_k) = \alpha + \beta + T * H * D + \gamma + \delta_{lineID} + \epsilon \quad (19)$$

275 where environmental covariates: temperature (**T**), relative humidity (**H**) and density (**D**) are  
276 fitted as fixed effects.  $\beta$  is a two-level categorical fixed effect (inbred lines or population).  $\gamma$  is  
277 a two-level categorical fixed effect accounting for differences between the years of phenotyping  
278 measurements of the A6140 lineages.  $\delta \sim \mathcal{N}(0, \sigma^2)$  a random effect accounting for line identity  
279 within populations and  $\epsilon \sim \mathcal{N}(0, \sigma^2)$  the residual error.

280 Both male and inbreeding models were fit using the *lmer* function in R package *lme4*, and non-  
281 zero values of fixed effects were tested against null models without fixed effects with likelihood  
282 ratio tests. Marginal  $r^2$  for the male frequencies were computed using the *r.squaredGLMM*  
283 function of the package *MuMIn* (Bartoń, 2020).

## 284 3.5 Transition rate genetics

### 285 3.5.1 **G**-matrix estimation

286 Genetic (co)variances of transition rates per population are estimated as half the between inbred  
287 line differences for lines separately derived from the evolving outbred populations. In the ab-  
288 sence of selection during inbreeding and canceling of directional non-additive gene action, this  
289 broad-sense **G**-matrix obtained from inbred lines is an adequate surrogate for the additive **G**-  
290 matrix of outbreeding populations (Kearsey and Pooni, 1996; Lynch and Walsh, 1998). We test  
291 these assumptions (see below).



292 **G**-matrices for the six non-self transition rates  $q_k$  were estimated from trait values for the  
293 inbred lines derived from focal populations. We estimated **G**-matrices separately for each of  
294 the seven populations (A6140, CA[1-3]50, CA[1-3]100). The 6 transition rates  $q_k$  were fitted as a  
295 multivariate response variable  $y$  in the model:

$$y = \mu + T * H * D + L + B + e. \quad (20)$$

296 where the intercept ( $\mu$ ) and the environmental covariates: temperature (**T**), relative humidity (**H**)  
297 and density (**D**) were fitted as fixed effects. Environmental covariates were fitted individually  
298 and with all possible interactions. Each covariate was standardized to a mean of 0 and standard  
299 deviation of 1. Block effects (**B**) and line identities (**L**) were modeled as random effects and **e**  
300 was the residual variance. We then estimated a matrix of genetic (co)variance as half the line  
301 covariance matrix (**L**). An additional two-level categorical effect was included when estimating  
302 the A6140 matrix that accounts for differences between the 2012 and 2013 phenotyping blocks in  
303 the first common garden. As mentioned above, a second A6140 matrix was computed from the  
304 data collected in the third common garden using the same model.

305 For modeling we use the R package *MCMCglmm* (Hadfield, 2010). We constructed priors  
306 as the matrix of phenotypic variances for each trait. Model convergence was verified by visual  
307 inspection of the posterior distributions and by ensuring that the autocorrelation remained below  
308 0.05. We used 100000 burn-in iterations, a thinning interval of 2000 and a total of 2100000 MCMC  
309 iterations.

### 310 3.5.2 *G*-matrices under random sampling

311 For each of our seven populations (A6140, CA[1-3]50, CA[1-3]100), we constructed 1000 ran-  
312 domised **G**-matrices to generate a null distribution against which to compare the observed esti-  
313 mates. We randomly shuffled both the inbred line and block identities and fit equation 20. We  
314 then computed the posterior means of our 1000 models to construct a null distribution.

315 We additionally generated 1000 matrices for the A6140 population using the same procedure  
316 on random subsets of 60 (of 188 total) inbred lines to determine the effects of sampling the same  
317 number of lines as those for CA[1-3]50 and CA[1-3]100 populations.

### 318 3.5.3 *G*-matrix divergence and differentiation

319 To compare the overall variance of the **G**-matrices during experimental evolution, we first com-  
320 puted the trace of the matrices and then performed spectral analyses of the posterior ancestral  
321 **G**-matrices. The decomposition of the posterior ancestral **G**-matrices allows one to describe the  
322 overall **G**-matrix shape, with the relative genetic variance between the six eigenvalues of each  
323 eigenvector, indicating whether the matrix is elliptical (a few large eigenvalues) or round (homo-  
324 geneous eigenvalues). The first eigenvector (defined as  $g_{max}$ ) is the linear combination of traits  
325 where the genetic variance is maximized.

326 We used eigentensor analysis to explore differences between the **G**-matrices, following Aguirre  
327 et al., 2014; Hine et al., 2009). Genetic (co)variance tensors ( $\Sigma$ ) are fourth-order objects describing  
328 how phenotypic dimensions between transition rates maximize differences between all the **G**-  
329 matrices. The genetic variation among multiple **G**-matrices can be described by  $\Sigma$  decomposition  
330 into orthogonal eigentensors ( $E_i$ , with  $i$  being the orthogonal dimensions), each associated with  
331 an eigenvalue quantifying its contribution to variation in  $\Sigma$  ( $\alpha_i$ ). In turn, eigentensors can be  
332 decomposed into eigenvectors ( $e_{ii}$ ), each with associated eigenvalues ( $\lambda_i$ ). Aguirre et al. (2014)  
333 implemented this approach in a Bayesian framework using *MCMCglmm*, and Morrissey and  
334 Bonnet (2019) made an important modification to account for sampling where the amount of  
335 variance in  $\alpha_i$  is compared to an expected distribution by sampling a finite number of lines.

## 3.6 Selection on transition rates

### 3.6.1 Selection surface

The log-transformed, covariate-adjusted fertility values (best linear unbiased estimates) for each inbred line were downloaded from Noble et al. (2017), exponentiated, and divided by the mean to obtain a relative fitness measure ( $w_l$ ).

Since we did not observe any directional change in locomotion behavior or component transition rates during lab evolution, and because the inbred lines were derived after domestication, most of adaptation to the lab environments has occurred, and we do not expect linear (directional) selection to be significant (but see below). We estimated quadratic selection gradients using partial regression, following (Lande and Arnold, 1983), with the *MCMCglmm* R package:

$$w_l = \alpha + \sum_{k=1}^6 \gamma_k z_{k,l}^2 + \sum_{k_1=1}^5 \sum_{k_2=k_1+1}^6 \gamma_{k_1,k_2} z_{k_1,l} z_{k_2,l} + \epsilon \quad (21)$$

with  $\alpha$  being the mean relative fitness among all lines and  $\gamma$  the partial coefficients estimating quadratic selection on each transition rate  $k$ , or between pairs of transition rates  $k_1$  and  $k_2$ . Environmental covariates (temperature, humidity, density) were defined and normalized as for the **G**-matrices estimation described above. Model residuals were normal and homocedastic (not shown).

We compared the results of this model (equation 21) with those of linear mixed effect models including as a random effect the additive genetic similarity matrix **A** between inbred lines, as defined in Noble et al. (2017) and Noble et al. (2019). We have also compared results from equation 21 to models including coefficients for linear selection on each transition rate. Under both circumstances parameter estimates are similar to those presented, albeit with changing credible intervals (not shown). Including other measured traits by the worm tracker, such as body size [a trait related to developmental time that is known to affect fertility in our populations (Theologidis et al., 2014)] similarly does not affect the qualitative conclusions we reach.

### 359 3.6.2 *G*-matrix alignment with the selection surface

360 We used canonical analysis (Phillips and Arnold, 1989) to visualize the selection surface as:

$$\Lambda = \mathbf{U}^T \boldsymbol{\gamma} \mathbf{U} \quad (22)$$

361 with  $\mathbf{U}$  being the matrix of eigenvectors of  $\boldsymbol{\gamma}$ , and  $\Lambda$  the diagonal matrix of eigenvalues  
362 (denoted  $\lambda_{[1-6]}$ ). **G**-matrices were rotated to visualize them as:

$$\mathbf{G}' = \mathbf{U}^T \mathbf{G} \mathbf{U} \quad (23)$$

363 To sample a null distribution of the  $\boldsymbol{\gamma}$  eigenvalues along the rotated dimensions, we fit the  
364 same model after permuting the relative fitness values of the lines. We then extracted the diago-  
365 nal elements of these permuted  $\boldsymbol{\gamma}$  after rotation using the estimated  $\mathbf{U}$ .

366 To see the evolution of the **G**-matrix in the selection surface, we calculated the Pearson prod-  
367 uct moment correlations between the eigentensor vectors explaining most of the genetic differ-  
368 ences between the 7 matrices ( $e_{11}, e_{12}$ ) with the canonical selection dimensions ( $y_1$ - $y_6$ ). We esti-  
369 mated uncertainty in these values by sampling from the posterior distribution of  $\boldsymbol{\gamma}$  1000 times.

## 370 3.7 Inference of effects

371 Most of our analysis relies on Bayesian inference of genetic or phenotypic effects. As discussed  
372 in Walter et al. (2018), the "significance" of effects can be inferred when there is no overlap  
373 between the posterior null sampling distributions with the posterior empirical estimate of the  
374 expected values. Thus, we compare expected value estimates such as a mean or mode with the  
375 95% credible intervals under random sampling of the expected value. The "significance" of the  
376 posterior mode estimates is based on their overlap with the posterior null distribution of the pos-  
377 terior modes (Walter et al., 2018). For all comparisons of posterior distributions significance can

378 be inferred when their 83% credible intervals do not overlap (Austin and Hux, 2002), assuming  
379 homoscedasticity.


380

## 4 Results

381

### 4.1 Laboratory culture

382 Our lab evolution system is based on a hybrid population derived from 16 founder strains  
383 (Figure 1A). Replicate samples from the hybrid population were domesticated for 140 non-  
384 overlapping generations at census size  $N=10^4$  to an environment in part characterized by constant  
385 density, temperature and relative humidity, and by little spatial structure during the life-cycle  
386 (see Methods). The dynamics of several life-history traits during domestication indicate that  
387 most adaptation to lab conditions occurred by generation 100 (Carvalho et al., 2014a,b; Poulet  
388 et al., 2016; Teotónio et al., 2012; Theologidis et al., 2014). From a single domesticated popula-  
389 tion we derived replicate populations and evolved them for another 100 generations in the same  
390 environmental conditions. Although we measured locomotion behavior throughout of lab evo-  
391 lution, we only follow the G-matrix of its component traits during the last 100 generations, after  
392 adaptation, a stage that we call here the focal stage of lab evolution (Figure 1A).

393  *C. elegans* reproduces mostly by selfing in nature though there is considerable variance in  
394 male mating performance among the founders (Teotónio et al., 2006). By training a model on  
395 a suite of size- and locomotion-related metrics, we found that hermaphrodites could be clearly  
396 differentiated from males (see Methods), and estimated males frequencies were high during the  
397 entire experiment (Figure S1). Because *C. elegans* are androdioecious, and hermaphrodites cannot  
398 mate with each other, average expected selfing rates at a generation are 1 minus twice the male  
399 frequency at the previous generation (Teotónio et al., 2012), and we can conclude that outcrossing  
400 was the predominant reproduction mode during lab evolution. Previously, we showed that  
401 effective population sizes during domestication were of about  $N_e=10^3$  (Chelo and Teotónio, 2013).

## 4.2 *Evolution of locomotion behavior*

We measured locomotion behavior at the time of reproduction for each outbred population and the inbred founders using worm video tracking (Swierczek et al., 2011). The output, after quality control and initial analysis, are individual worm tracks categorized at a given point in time by activity (moving, or not) and direction (forwards or backwards). We model a three-state memoryless (Markov) process with homogeneous spatial and temporal dynamics (see Methods, Figure S2). We view this as an obviously false but useful approximation of worm locomotion behavior under our conditions, which is only partially violated (worms tend to resume forward movement more often than expected; Figure S3). Component traits of locomotion behavior are the (sex-specific) six non-self transition rates between forward movement, backward movement, and immobility.

We find that while the founders of lab evolution show great diversity in locomotion behavior under lab conditions, evolved populations rapidly attained, and maintained, a stable level after hybridization for 240 generations. For example, considering the proportion of time individual worms are stationary (Figure 1B), we observe values of around 40% for hermaphrodites - much higher than most founders - while males are much more vagile (stationary around 10%). Neither hermaphrodite nor male transition rates showed a directional change from the hybrid ancestral state over the full 240-generation period (Table 1, Supplementary Figures S4 and S5). Differences between replicate populations can be explained by sampling error.

## 4.3 *Broad-sense G-matrix*

To estimate G-matrices, we used approximately 200 lines from the generation 140 domesticated population (A6140), and approximately 50 lines from each of three replicate populations derived from A6140 and sampled at generations 50 (CA[1-3]50) and 100 (CA[1-3]100) of the focal lab evolution. We use these broad-sense G-matrices as a surrogate for the narrow-sense (additive) G-matrices of the outbred populations (see Methods). These two kinds of matrices might not

427 be identical because of selection during inbreeding or because of differential expression of non-  
428 additive genetic effects in inbred and outbred individuals. Such differences, if present, manifest  
429 as differences in the mean values of inbred and outbred samples as directional effects will sta-  
430 tistically average out for polygenic traits (Kearsey and Pooni, 1996; Lynch and Walsh, 1998). We  
431 used the inbred lines and the focal A6140 ancestor to compare means for all transitions and we  
432 did not find any evidence of directional non-additive genetic effects (Table 2).

433 Our **G-matrices** could also differ from the **G-matrices** of outbred populations due to the  
434 absence of males in the inbred lines; which were abundant in the outbred populations. This is  
435 because males are known to disturb hermaphrodite locomotion behavior (Lipton et al., 2004).  
436 We tested for effects of male frequency on transition rates in outbred populations with univariate  
437 linear models and found that they were weak at best (Figure S6).

#### 438 4.4 *G-matrix evolution*

439 For the domesticated 140 population (A6140), ancestral to all CA populations during further 100  
440 generations in the same environment after adaptation, there is significant genetic variance in  
441 all hermaphrodite transition rates, relative to a null distribution from permutations of line and  
442 technical replicate identity (Figure 2A). Likewise, the posterior distributions of most (12 of 15)  
443 covariance estimates between transition rates do not overlap 0, and differ from the null distribu-  
444 tion of posterior means. The A6140 **G-matrix** is structured in two main behavioral modules, with  
445 the transitions from still to forward or backward (i.e. leaving the still state) showing positive  
446 covariances with each other and negative covariances with other transition rates.

447 Inbred lines from the ancestral and evolved populations at generation 50 and 100 were phe-  
448 notyped in separate common garden experiments. CA[1-3]50 inbred lines show a clear difference  
449 in all transition rates variance but also in mean body area or velocity (not shown) indicating that  
450 relative phenotypic values between CA[1-3] lines cannot be compared. We phenotyped A6140  
451 lines together with all CA[1-3]100 lines and ensured that these measurements were comparable  
452 (see Figure S9). Thus, we only compare **G-matrix** differentiation between A6140 and CA[1-3]100

453 populations but we discuss the divergence among the three CA[1-3]50 G-matrices as they were  
454 phenotyped in a single common garden.

455 When looking at the evolved CA populations, we see that their G-matrices are reduced af-  
456 ter 100 generations of evolution (Figure S7). Reduced genetic (co)variance in generation 100 is  
457 particularly obvious when calculating the trace of the G-matrices, although all populations con-  
458 tain more genetic variance than expected by chance (Figure 2B). The loss of genetic (co)variances  
459 during focal evolution could be due to differences in statistical power or the result of continued  
460 lab evolution. Sub-sampling A6140 to the sampling sizes of CA[1-3]100 populations, while in-  
461 creasing the credible intervals did not affect the estimated modes, with many of them remaining  
462 different from the null (Figure S8). This difference is robust to common garden variation (see  
463 Figure S9A).

464 Eigendecomposition of the A6140 G-matrix further shows that, for the phenotypic dimen-  
465 sion encompassing 64% of genetic variation in this population ( $g_{max}$ ), the projected variance of  
466 CA[1-3]100 populations in this dimension is much reduced (Figure 2C). In this  $g_{max}$  dimension  
467 of maximal ancestral variation, leaving the still movement states (still-to-forward, and still-to-  
468 backwards, transition rates) are positively associated with each other while being negatively  
469 associated with all other transition rates (Table 3).

#### 470 4.5 Genetic divergence and differentiation

471 We tested for divergence of the G-matrices from the ancestral state during 100 generations, and  
472 for differentiation between derived replicate populations at generation 50 using eigentensor anal-  
473 ysis (see Methods). This analysis identifies the phenotypic dimensions along which there are  
474 most differences between the several matrices being compared.

475 When looking for divergence between A6140 and CA[1-3]100, the first eigentensor,  $E_1$ , ex-  
476 plains more variation than the null expectation (Figure 3A, 73%). G-matrix coordinates in the  
477 space of  $E_1$  (Figure 3B), show that the A6140 population drives most significant differences  
478 between all matrices, and thus encompasses most of the genetic divergence. Along the first



479 eigenvector of  $E_1$  (called  $e_{11}$ ; Figure 3C) divergence is due to loss of genetic variance in the CA  
480 populations. We further find that  $e_{11}$  is highly collinear with the  $g_{max}$  of the A6140 population,  
481 the phenotypic dimension encompassing most ancestral genetic variation (not shown). Simi-  
482 lar results were found when comparing the A6140 results from the third common garden with  
483 the CA[1-3]100 populations, ensuring that the assay period does not affect the mean variance  
484 estimates (see Figure S9).

485 We tested for differentiation between replicate populations during focal evolution by restrict-  
486 ing the spectral analysis to only the three CA[1-3] G-matrices, separately at generation 50 and  
487 generation 100. For the CA[1-3]50 populations, we observe that a single eigentensor was differ-  
488 ent from the null expectations, explaining 53% of the differences between the three G-matrices  
489 (Figure S10). The coordinates of these matrices in the space of the eigentensor indicate that  
490 CA150 and the remaining two populations contributed in opposite directions to the difference  
491 observed. Most of this difference is expressed along the first two eigenvectors (50% and 37%):  
492 CA[2-3]50 lost variance along the first eigenvector and CA150 along the second one. A similar  
493 analysis at generation 100 did not show differentiation between the three CA[1-3]100 G-matrices  
494 (not shown).

#### 495 4.6 Selection on locomotion behavior

496 In Noble et al. (2017) we reported the fertility of many of the inbred lines used to estimate the  
497 G-matrices. This data encompasses hermaphrodite self-fecundity and progeny viability until  
498 early larvae, measured in an environment that closely mimicked that of lab evolution. With  
499 this data at hand we can estimate the selection surface of locomotion in our lab environment  
500 by applying equation 21, with relative fertility being partially-regressed onto the transition rates  
501 (see Methods).

502 We find that the 95% credible intervals for several coefficients for correlated selection between  
503 pairs of transition rates do not overlap zero: negative between still-forward (SF) and forward-  
504 still (FS) and positive between SB and FS, and FS and BS (Figure S11). To visualize the selection

505 surface, we rotated the  $\gamma$ -matrix with canonical analysis (see Methods). The resulting selection  
506 surface suggests a saddle with three unstable equilibria in three canonical dimensions  $y_1$ - $y_3$ ,  
507 indicating disruptive selection, and three stable equilibria in three dimensions ( $y_4$ - $y_6$ ), indicating  
508 stabilizing selection (Figure 4, Table 4). We only find, however, evidence of weak and strong  
509 stabilizing selection on  $y_5$  and  $y_6$ , respectively, because only these empirical estimates are unlikely  
510 under the null distribution.

#### 511 4.7 *G*-matrix evolution in the selection surface

512 Projection of the *G*-matrices onto the canonical selection dimensions shows that most genetic  
513 variance is concentrated in dimension  $(y_3, y_4)$ , while the dimensions under stabilizing selection  
514 ( $y_5$  and  $y_6$ ) do not show much genetic variance that can be lost after generation 140 (Figure 5).  $y_1$   
515 does similarly not show much genetic variance. Along all selection dimensions, loss of genetic  
516 variance is consistent with drift when assuming an infinitesimal model of trait inheritance (Barton  
517 et al., 2017) and effective population sizes of  $N_e = 10^3$  (Chelo and Teotónio, 2013). For the  $y_1$   
518 and  $y_6$  dimensions, initial and evolved populations at generation 100 clearly varied less than the  
519 founders isolates of experimental evolution, as their 83% posterior distributions do not overlap.

520 To assess if *G*-matrix evolution aligned with the selection surface, we calculated the correla-  
521 tion between the directions of genetic divergence at generation 100 of the focal stage (Figure 3),  
522 and differentiation of replicate population at generation 50 (Figure S10), with the canonical se-  
523 lection dimensions (Figure 4). Overall there is a strong alignment of both divergence and differ-  
524 entiation axes with  $y_3$  (Figure S12), and thus with  $g_{max}$  (see above).

## 525 5 Discussion

526 The evolution of *C. elegans* locomotion behavior during 240 generations in a fairly constant and  
527 homogeneous lab environment is characterized by stasis, following a genetically and pheno-  
528 typically dynamic 33 generation period of hybridizing the founder strains. Most of the genetic

529 variance along the several phenotypic dimensions under stabilizing selection or drift was lost,  
530 suggesting directional selection during the hybridization of founders and domestication until  
531 generation 140. Despite phenotypic stasis, genetic divergence and differentiation continued dur-  
532 ing further 50 to 100 generations of evolution in the same environment, a result that is sufficiently  
533 explained by drift. These results suggest that directional selection outside a local phenotypic  
534 space after adaptation ensures phenotypic stasis and that over a larger phenotypic space there  
535 was effective stabilizing selection. A future venue for research in our experimental system is to  
536 find if specific mechanisms of density and/or frequency-dependent selection – such as sex allo-  
537 cation, sexual selection, viability selection during early larval growth, maternal effects, etc.; as we  
538 before described in some of the same populations (Carvalho et al., 2014b; Chelo et al., 2013; Dey  
539 et al., 2016; Pouillet et al., 2016) –, underlie effective stabilizing selection on locomotion behavior.  
540 It would further be interesting to test if starting lab evolution from founders whose average loco-  
541 motion behavior is away from the phenotypic space measured in our populations converge into  
542 a similar “adaptive zone” cf. (Simpson, 1944; Uyeda et al., 2011), or are constrained by standing  
543 genetic variation.

544 The loss of genetic variance from the 16 founders to the domesticated population in the se-  
545 lection surface dimensions  $y_1$  and  $y_6$  is notable because it suggests that the rapid phenotypic  
546 evolution during intercrossing of founders to form the hybrid population was due to initially  
547 strong directional selection, which subsequently weakened during lab domestication. It can be  
548 argued that, with only 16 founders, we have little power to reject the hypothesis that there was  
549 no loss, and that the genetic (co)variances we found after domestication simply reflect natural  
550 standing genetic variation. At mutation-drift balance, the **G-matrix** should reflect the patterns  
551 of mutational effects described by the **M** matrix, the equivalent measure of trait mutational vari-  
552 ances, and covariances between them due to pleiotropy (Lande, 1979; Lynch and Hill, 1986).  
553 Elsewhere, we have estimated the **M** matrix in two of the founders of lab evolution, which show  
554 locomotion values divergent from those of lab evolution populations, by phenotyping a set of  
555 about 120 lines that accumulated mutations in a nearly-neutral fashion for 250 generations (Baer

556 et al., 2005; Yeh et al., 2017). We found that the **M** matrices from these founders have similar  
557 sizes and are well aligned with each other, but not with the genetic **G-matrix** of our A6140 do-  
558 mesticated population (Mallard et al., 2022b). Loss of genetic variances from the founders during  
559 hybridization and lab domestication was therefore at least partly due to directional selection. Fu-  
560 ture work should nonetheless try to understand if mutation-selection balance is responsible for  
561 the maintenance of genetic variation in locomotion behavior in nature by comparing **G-matrices**  
562 from natural populations, as they can be obtained from a large collection of wild isolates now  
563 available (Cook et al., 2017; Lee et al., 2021), with **M** matrices (Houle et al., 1996; Johnson and  
564 Barton, 2005).

565 We did not find a change in genetic variance along the phenotypic dimension of strong stabi-  
566 lizing selection ( $y_6$ ) because by generation 140 there was already little variation in this dimension.  
567 More genetic variance than expected by drift on  $y_6$  was expected because QTL mapping of the  
568 selection trait  $y_6$ , using the sequence data of Noble et al. (2019) subset of the inbred lines,  
569 detects two QTL with high minor allele frequencies ( $> 30\%$ , not shown). We also previously  
570 shown that until generation 100 after founder hybridization excess heterozygosity was main-  
571 tained relative to that expected under drift and linked selection on deleterious recessives (Chelo  
572 et al., 2019; Chelo and Teotónio, 2013). The methods employed here were clearly under powered  
573 to detect genetic variance. We cannot rule out, however, the strength selection was  
574 overestimated or that estimates are not biased about the form of selection because environmental  
575 covariances with unmeasured traits could have caused correlated selection with transition rates  
576 (Blows and Brooks, 2003; Hunt et al., 2007; Mallard et al., 2022a). A perhaps more serious concern  
577 is the role of unmeasured traits under potential selection that might be genetically correlated with  
578 the observed transition rates (Barton and Turelli, 1987; Lande, 1979; Mallard et al., 2022a; Shaw  
579 et al., 1995). Modeling additive genetic similarity among the inbred lines used in the regression  
580 (Noble et al., 2017, 2019) does not qualitatively change the inference about selection on transition  
581 rates (not shown), though we did not model the genetic architecture of locomotion behavior with  
582 multiple traits as the dependent variables. Several models have proposed that pleiotropic effects

583 on unmeasured traits, which we did model, could explain maintenance of genetic variation in  
584 quantitative traits, though under weak selection and close to linkage equilibrium between QTL  
585 alleles in the long term of mutation-selection balance (Barton, 1990; Johnson and Porter, 2007;  
586 Simons et al., 2018; Zhang and Hill, 2005). While in our case transition rates between movement  
587 states should define the overall locomotion behavior of *C. elegans*, we cannot dismiss that genetic  
588 covariation with unmeasured traits will better predict the evolution of genetic variances along  
589 the selected phenotypic dimensions.

590 One of the major findings here is that of divergence and transient differentiation of the **G-**  
591 **matrix** during the last 100 generations of lab evolution. The phenotypic dimensions of genetic  
592 divergence and differentiation among all populations were not aligned with the phenotypic di-  
593 mensions under selection, and most if not all of the genetic variance lost during this focal 100-  
594 generation period was expected with drift. Not unexpectedly, loss of genetic variance mostly oc-  
595 curred along the dimensions with most genetic variance in the ancestral lab-adapted population  
596 ( $g_{max}$ ). It is possible that this dimension represents a continuum between activity and direction  
597 of movement in foraging and dwelling, expressed by the positive association between transition  
598 rates from the still state (Flavell et al., 2020; Gray et al., 2005). Stabilizing selection favors a nega-  
599 tive association between transition rates from the still state, which, elsewhere, we have shown is  
600 under directional selection in a new stressful environment (Mallard et al., 2022a). As was the case  
601 here, however, transition rates from the still state in the new stressful environment did not evolve  
602 under directional selection because of a lack of relevant genetic variation in the appropriate di-  
603 rection. Overall, these observations are congruent with those of experiments in *D. melanogaster* by  
604 Fowler and colleagues where, after bottlenecking an outbred population, there was a reduction  
605 in the size of the **G-matrix** for wing morphology in the derived bottlenecked populations, and  
606 size divergence among them, as expected under drift (Fowler and Whitlock, 1999; Phillips et al.,  
607 2001). Genetic divergence also occurred because the shape of the **G-matrix** changed as derived  
608 populations showed different genetic covariances between traits. Interestingly, drift history was  
609 consequential to the future phenotypic divergence of particular bottlenecked populations in a

610 new environment (Whitlock et al., 2002). We suspect that a similar result would have been ob-  
611 served had we performed experimental evolution in a new environment and having as ancestral  
612 populations the differentiated replicates from generation 50 of the focal stage.

613 Most of our analyses and the underlying theoretical predictions are predicated on the as-  
614 sumption that the infinitesimal model of trait inheritance is a good approximation of the truth.  
615 However, that assumption may be violated, inasmuch as the genetic variances and covariances  
616 of locomotion behavior will not on the short-term of our hybridization and lab evolution be in-  
617 dependent of allele frequency changes and linkage disequilibrium between smaller effect quan-  
618 titative trait loci (QTL). QTL allele frequency independence is expected only in the long-term  
619 when approaching strong recombination and weak selection, mutation and drift, steady-states  
620 (Barton, 1990; Barton et al., 2017; Vladar and Barton, 2014). Our findings pose the question of  
621 how genetic drift, together with effective stabilizing selection, generates variable allele frequency  
622 changes at QTL so that pleiotropy or linkage disequilibrium between them eventually results in  
623 genetic covariances that diverge from the ancestral states and are not common among replicate  
624 populations. Even if eventually populations lose most genetic variance, this transient differentia-  
625 tion could be important for future phenotypic evolution were the environment to change. In our  
626 case, recombination during the focal stage should have remained much weaker than selection  
627 between 0.5-1 cM regions (Chelo and Teotónio, 2013; Noble et al., 2017, 2019); for total a total  
628 genome size of 300 cM. If after domestication several QTL alleles within these linked regions  
629 segregate at low frequency, it is possible that selection and drift was such that each replicate  
630 population during divergence fixed alleles with differently signed phenotypic effects that would  
631 not average out when comparing across populations (Bernstein et al., 2019; Cohan, 1984; Gromko,  
632 1995). Inflation of the effects of drift is further expected because there is a correlation across gen-  
633 erations between the traits' breeding values of successful parents and their offspring, resulting in  
634 a reduction in effective population sizes (Robertson, 1961; Santiago and Caballero, 1998).

635 Short-term phenotypic stasis without genetic divergence in natural populations has been ex-  
636 plained by indirect selection or phenotypic plasticity, among several other processes cf. (Estes

637 and Arnold, 2007; Pujol et al., 2018), despite heritability and direct selection on the traits that  
638 were followed. Our study shows that phenotypic stasis can also occur with simultaneous genetic  
639 divergence and transient genetic differentiation. We conclude that the adaptive landscape in our  
640 lab environment is best understood as a table-top mountain, where a saddled plateau with dif-  
641 ferent optima are of little consequence to genetic or phenotypic divergence. Outside the plateau,  
642 directional selection explains phenotypic stasis and loss of genetic variation, within the plateau  
643 drift appears to be the main driver of evolution. In the long-term, phenotypic stasis is a common  
644 pattern observed over periods of up to a million years. For longer periods, rapid divergence in  
645 mean trait values is observed from fossil records, or inferred from phylogenetic trees, potentially  
646 because new adaptive zones are accessible after extreme ecological changes. Given our results,  
647 we speculate that upon such changes, phenotypic divergence and differentiation of populations  
648 can be facilitated by cryptic evolution of genetic covariance structure during phenotypic stasis.  
649 In the short term, our study indicates that the combined effects of genetic drift and selection on  
650 the genetic covariance structure of multiple traits should be analytically modeled to understand  
651 phenotypic stasis better.

## 622 **6 Acknowledgments**

653 We thank A. Crist, J. Garcia, H. Gendrot, C. Goy, V. Pereira, F. Melo, and A. Silva for help with  
654 worm handling and data acquisition; R. Costa, R. Kerr, and N. Scwierczek for help with hardware  
655 and software implementation; N. Barton, C. Dillmann, A. Futschik, L. Kollar, S. McDaniel, P.  
656 Phillips, S. Proulx, A. Le Rouzic, and A. Veber for discussion. We also thank the anonymous  
657 reviewers that greatly improved the presentation of this work.

## 658 **7 Funding**

659 This work was supported by the European Research Council (ERC-St-243285) and the Agence Na-  
660 tionale pour la Recherche (ANR-14-ACHN-0032-01, ANR-17-CE02-0017-01) to HT, the National

661 Institutes of Health (R01GM107227) to CB, and a Marie Curie fellowship (H2020-MSCA-IF-2017-  
662 798083) to LN. This research has also received support, under the KITP Quantitative Biology  
663 program, from the National Science Foundation (PHY-1748958) and from the Gordon and Betty  
664 Moore Foundation (2919.02).

## 665 **8 Author contributions**

666 Conceptualization FM, LN, CB, HT; hardware and software implementation BA, TG; data acqui-  
667 sition and analysis BA, FM, LN, TG; funding acquisition LN, CB, HT; project administration HT;  
668 resources CB, HT; writing, original draft FM, HT; writing, review and editing LN, CB; correspon-  
669 dence FM (mallard@bio.ens.psl.eu) and HT (teotonio@bio.ens.psl.eu).



## 9 Figures

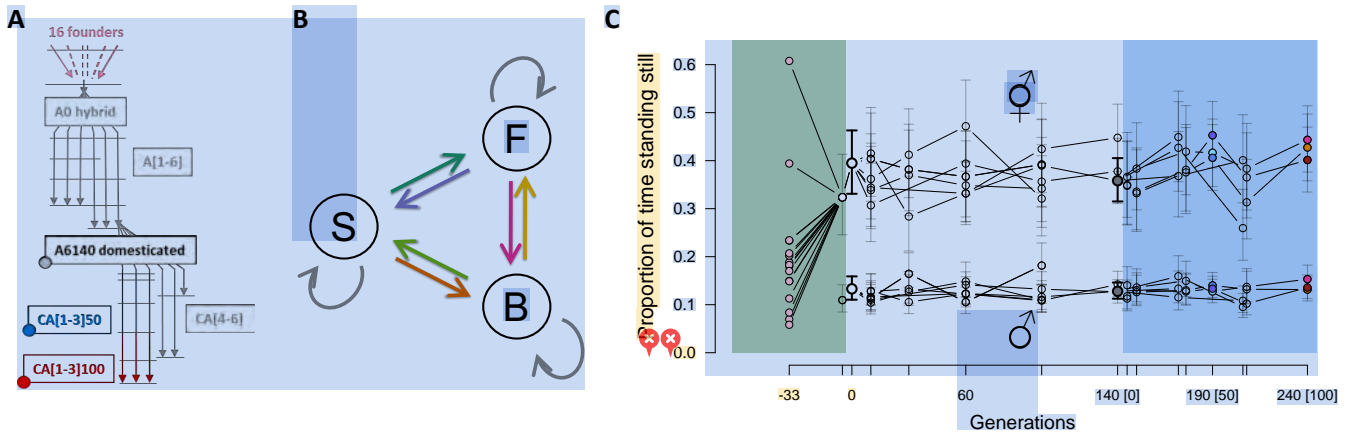


Figure 1: **A.** Experimental design. One hybrid population (A0) was created from the intercross of 16 inbred founders. Six replicate populations were then domesticated to a defined lab environment and after 140 generations one of these (A6140) was the ancestor to six other replicate populations maintained for an extra 100 generations under similar conditions (CA). Inbred lines were derived by selfing hermaphrodites (colored circles) from A6140 and three replicate CA populations [CA[1-3]50 and CA[1-3]100] at generation 50 and 100 (blue and red). Horizontal lines indicate outbred population samples that were phenotyped. **B.** Modelling locomotion behavior from component traits, defined by the transition rates between moving forward (F), moving backward (B) or being stationary (S). We consider the 6 independent non-self rates, shown in colored arrows. **C.** Evolution of locomotion behavior. Stationary frequency in the founders (pink dots) and outbred populations during lab evolution. Colored overlays indicate three stages of lab evolution: hybridization, domestication and focal. Ticks are sampled time points, while colored points during the focal stage indicate populations from which inbred lines were derived. Point mean estimates are shown for 3-6 replicate populations at other generations, with 95% confidence intervals for each one of them. The evolution of the component traits of locomotion behavior in hermaphrodites and males, the transition rates between movement state and direction, can be found in Figures S4 and S5.

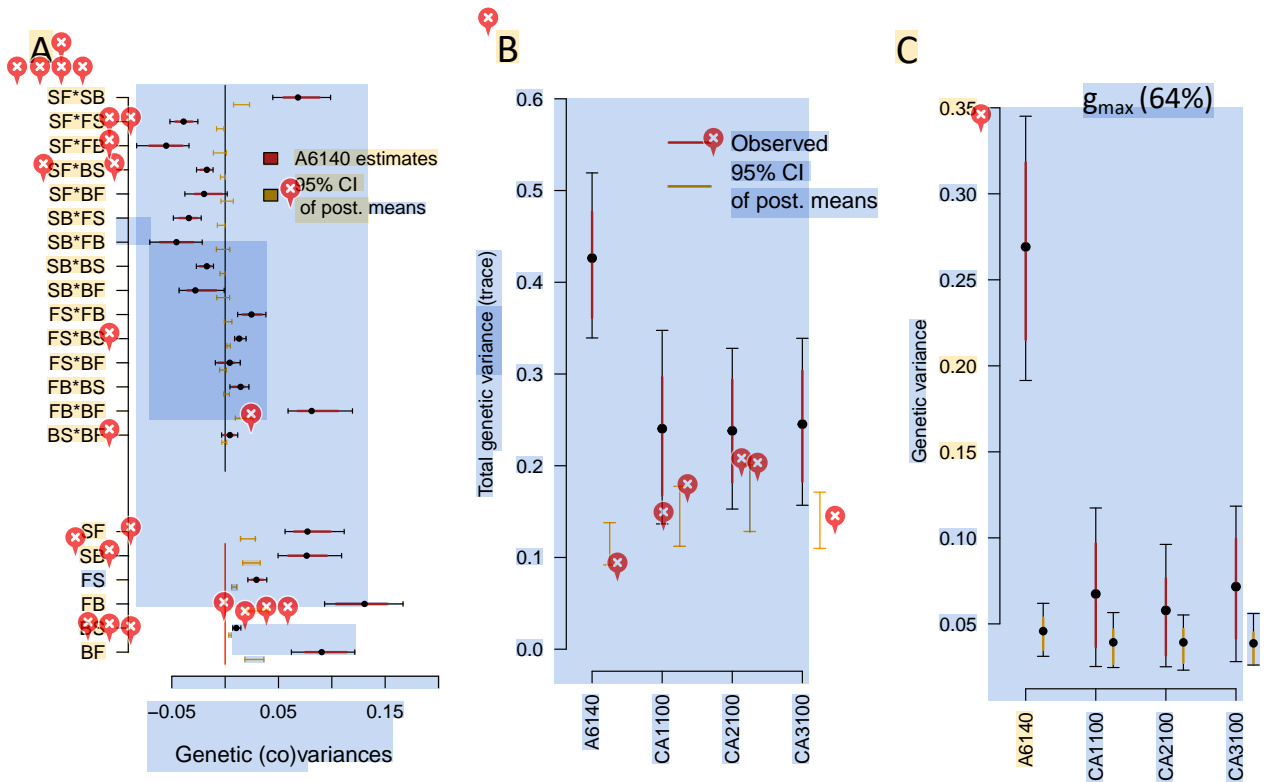


Figure 2: **G**-matrix evolution during the focal stage. **A.** A6140 **G**-matrix. Shown are the 15 genetic covariances between transitions rates (top) and six the genetic variances of transition rates (bottom), as bars and dots the 95% and 83% credible intervals (black and red) and mean of the posterior distribution, respectively. "S", "F", "B" stand for still, forward and backward movement states, with letter ordering indicating the direction of movement. **G**-matrices of the CA populations can be found in Supplementary Figure S7. **B.** Total amount of genetic variance computed as the sum of the **G** diagonal elements (trace). All observed posterior means differ from the null 95% of posterior means (orange). **C.** Genetic variance along the phenotypic dimension encompassing most genetic variation ( $g_{max}$ , red mean, 83% and 95% CI), when spectral decomposition is done on A6140 and CA[1-3]100 variances on this A6140  $g_{max}$  dimension is calculated. A6140  $g_{max}$  explains 64% of the total genetic variance. See ?? for the eigendecomposition results for the A6140 population.

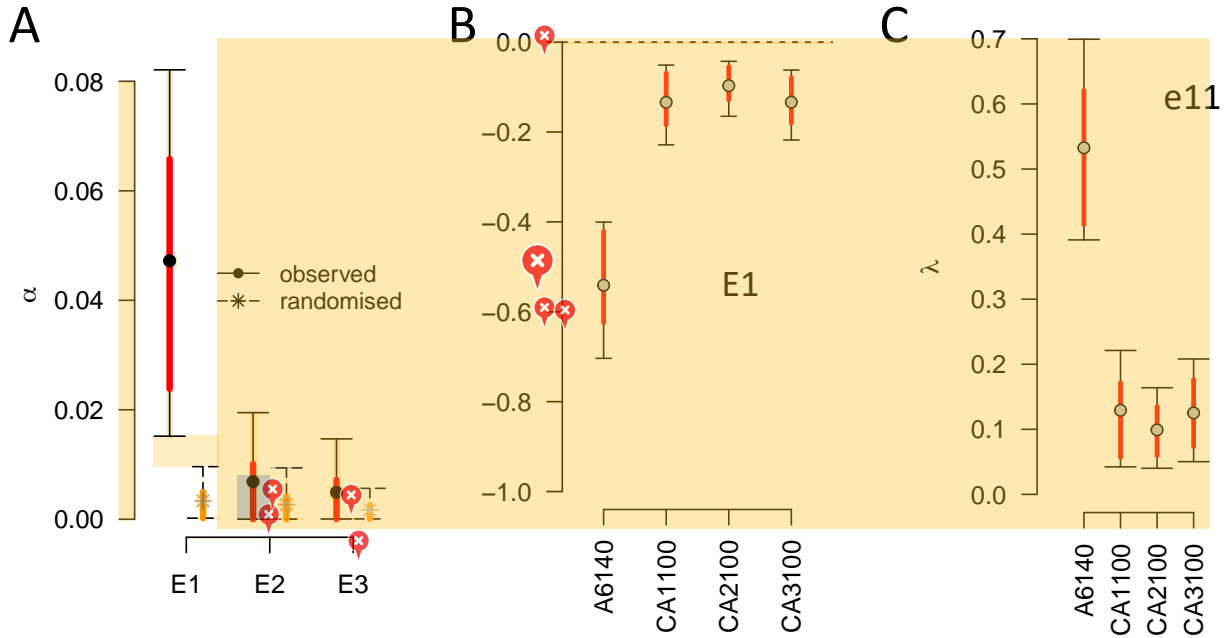


Figure 3: Genetic divergence. **A.** Spectral decomposition of variation among **G**-matrices. The variance  $\alpha_i$  associated with the  $i$ th eigentensor  $E_i$  is compared to a null permutation model where variation among matrices is due to sampling (see Methods). Although several eigentensors are different from zero (black bars, 95% credible interval) only the first one,  $E_1$ , do not overlap the null (red and orange bars, 83% credible intervals). **B.** The coordinates of the **G**-matrices in the space of the first eigentensor  $E_1$  for each population tested. Absolute values of the coordinates in the first eigentensor represents its contribution to the difference between matrices. **C.** Contribution of specific transition rate combinations to coordinated changes among **G**-matrices. The amount of genetic variance in the direction of the greatest variation among all **G**s for the first eigenvector of  $E_1$  ( $e_{11}$ ), for each population. Eigentensor decomposition of the CA[1-3]50 **G**-matrices, testing for differentiation at generation 50, can be found in [Figure S9](#).

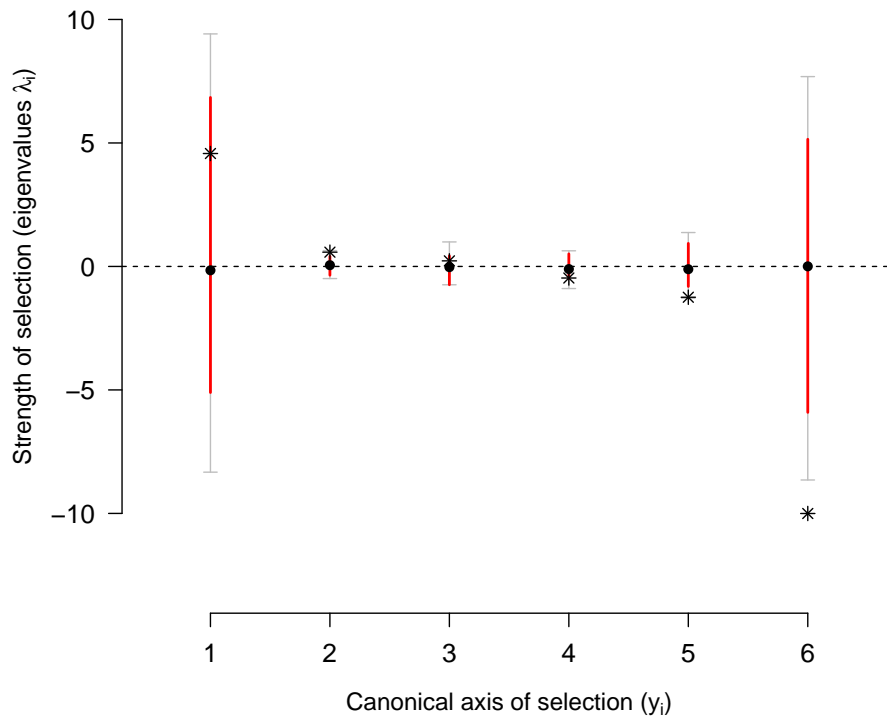


Figure 4: Selection surface of locomotion behavior. Canonical analysis of the  $\gamma$ -matrix shows positive phenotypic dimensions ( $y_1$ - $y_3$ ) of transition rate combinations under disruptive selection (as measured by the eigenvalue  $\lambda$ ), and negative dimension ( $y_4$ - $y_6$ ) under stabilizing selection. Stars show the mode of the posterior empirical distribution (see Methods). These estimates are to be compared to the posterior distribution of null modes (dots and colored bars, the mean and 83% and 95% credible intervals). The  $\gamma$ -matrix before canonical rotation can be found in [Figure S11](#).

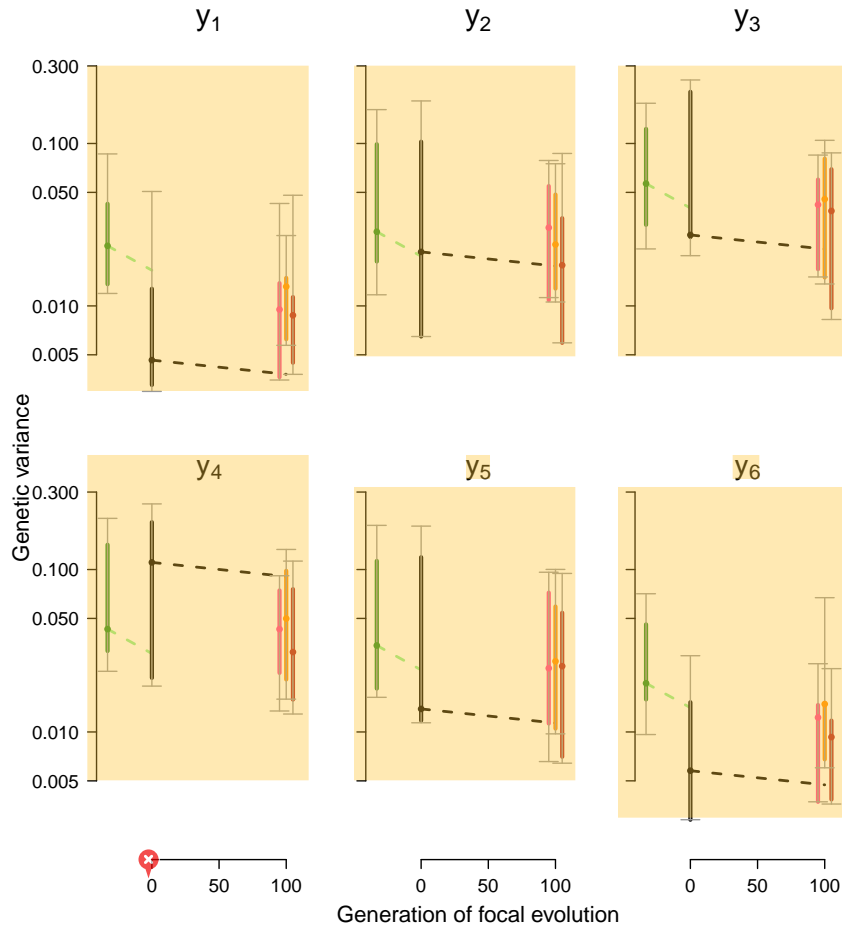


Figure 5: **G-matrix** evolution in the selection surface. Loss of genetic variance along axes  $y_2$ - $y_5$ , which contain most of the genetic variance in the evolved populations and are under very weak or no selection, is compatible with expectations from genetic drift under the assumption of **infinitesimal** trait inheritance (dashed lines, for  $N_e = 10^3$ ). Along  $y_1$  and  $y_6$ , genetic variance was much reduced relative to the founders of experimental evolution (**green**). The genetic variance of each canonical axis  $y_i$  was obtained by rotation of the original **G**-matrices, with 95% (grey) and 83% (colored) credible intervals from sampling 400 matrices in the posterior distributions for each **G**-matrix. Dots show the median estimates.

## 10 Supplementary Figures

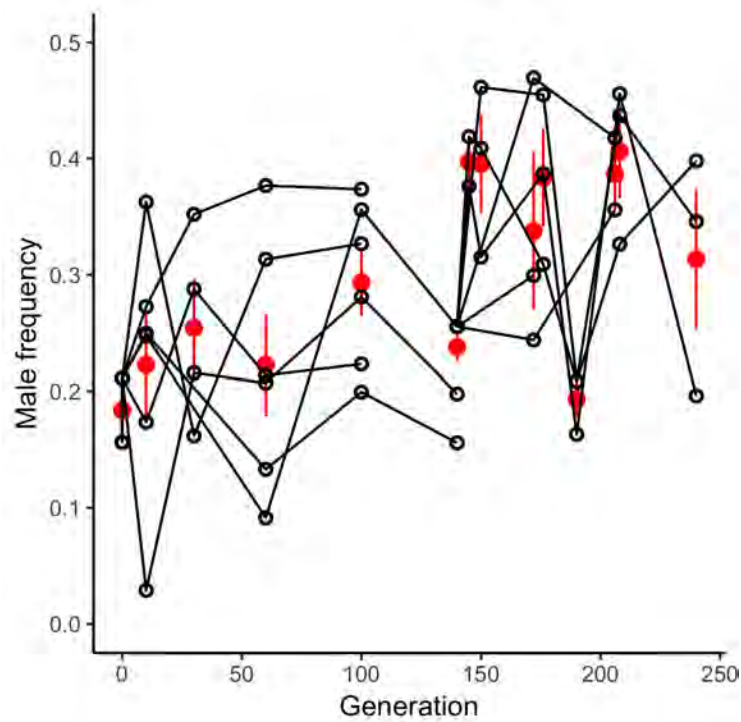


Figure S1: Male frequencies during lab evolution. Males and hermaphrodite tracks were differentiated with a 30-trait classifier based on moments of size, shape and velocity-related traits derived from Multi-Worm Tracker metrics, and frequencies were estimated from 1s slices across movies. Empty circles indicate the estimates for each replicate population (between 1 and 6 at each time point), red circles the mean among replicate populations ( $\pm$  standard error). During the first 100 generations of domestication, the estimates are similar to those obtained by directly counting the number of males (Teotónio et al., 2012).

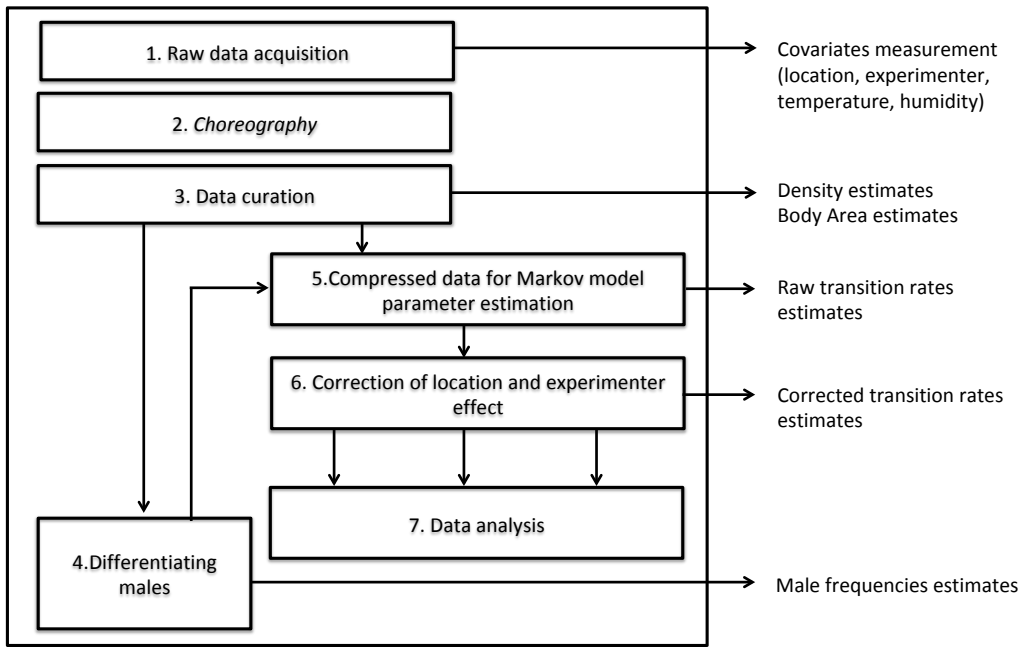


Figure S2: Schematic of data acquisition and analysis pipeline.



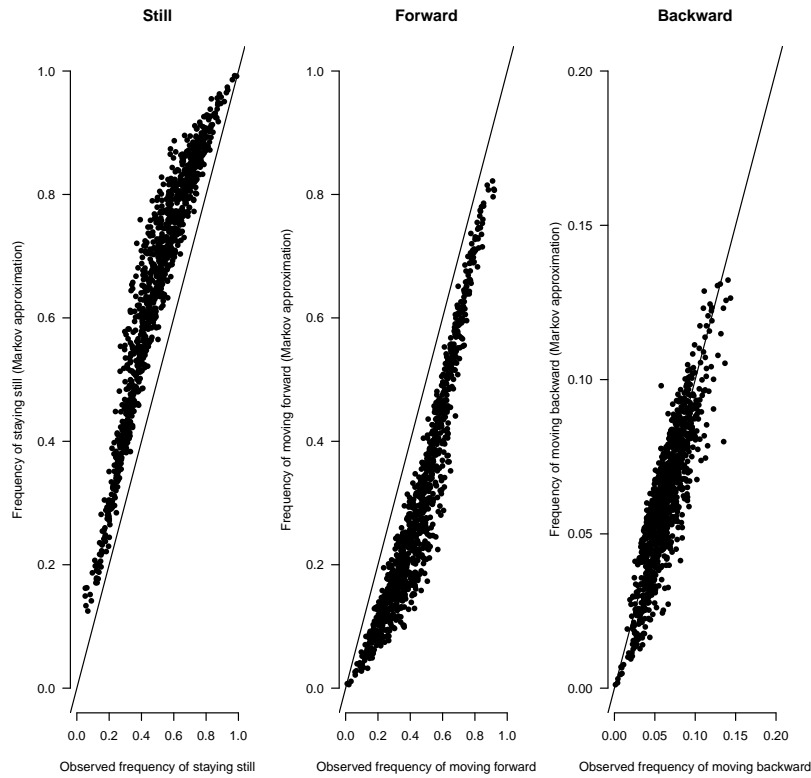


Figure S3: Correlation between the observed frequencies of each of the three movement states and the predicted values from the Markov model. There is a consistent bias in the long term predictions due to violation of the memoryless assumption of the model. Some moving worms tend to remain in this state longer than expected on the long term, that is, they can be briefly interrupted but are more likely to resume movement than predicted.

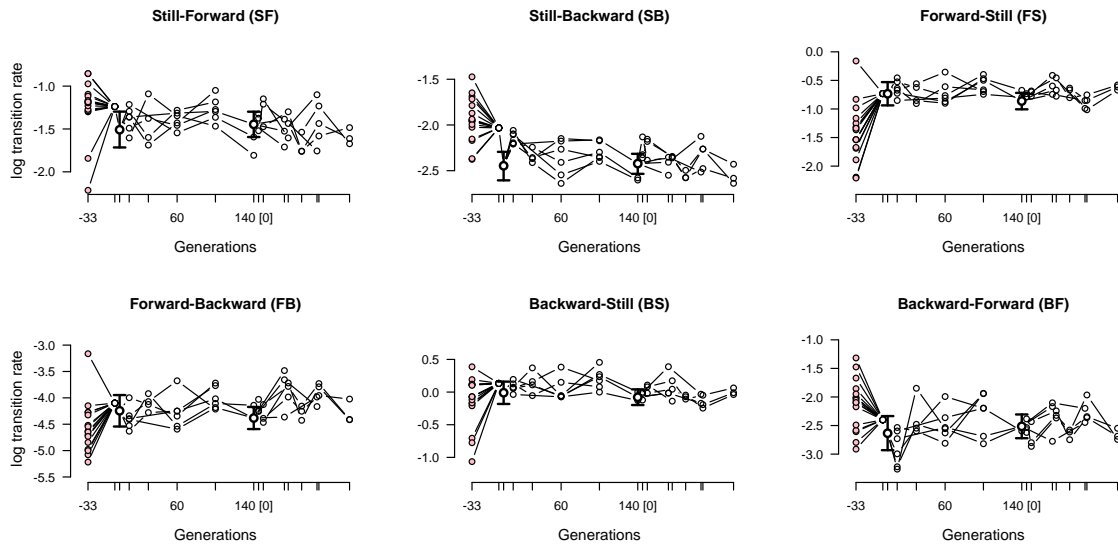


Figure S4: Evolution of mean hermaphrodite transition rates. Each panel shows the evolution of a transition rate in the founders (pink dots) and during experimental evolution (white dots). At the beginning of the domestication and focal stages there was one ancestral population, shown by empty circles with 95% credible intervals, while 3-6 replicate populations were measured at each sampled time point indicated by tick marks.

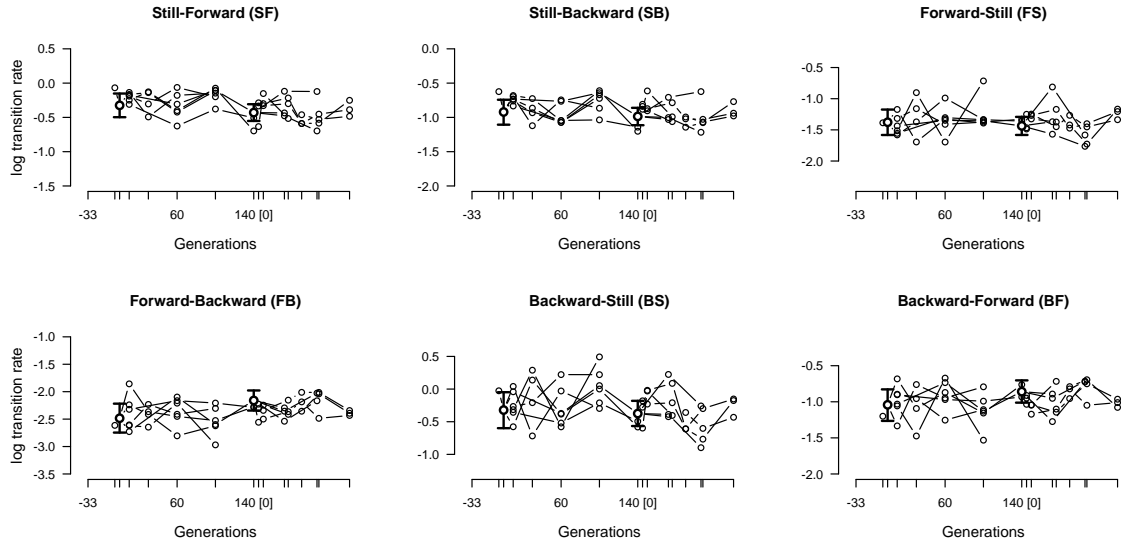


Figure S5: Evolution of mean male transition rates, as in [Figure S4](#). Note that the founder inbred lines do not have any males.

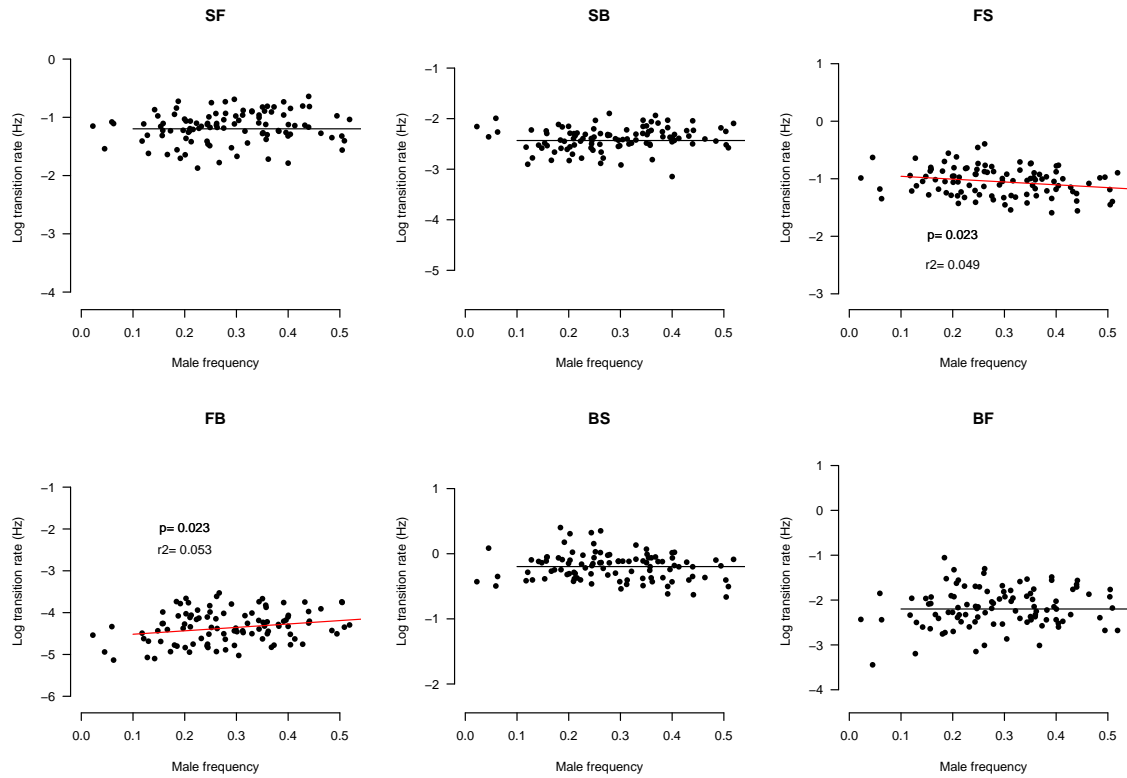


Figure S6: The effects of males on hermaphrodite transition rates in the outbred populations during lab evolution. Each point shows the relation between transition rates and male frequency for each replicate population at a given time point during lab evolution. Red (black) lines show significant (non-significant) linear effects of male frequency on transition rates. For all regression models the coefficient of determination is extremely low ( $r^2$ ).



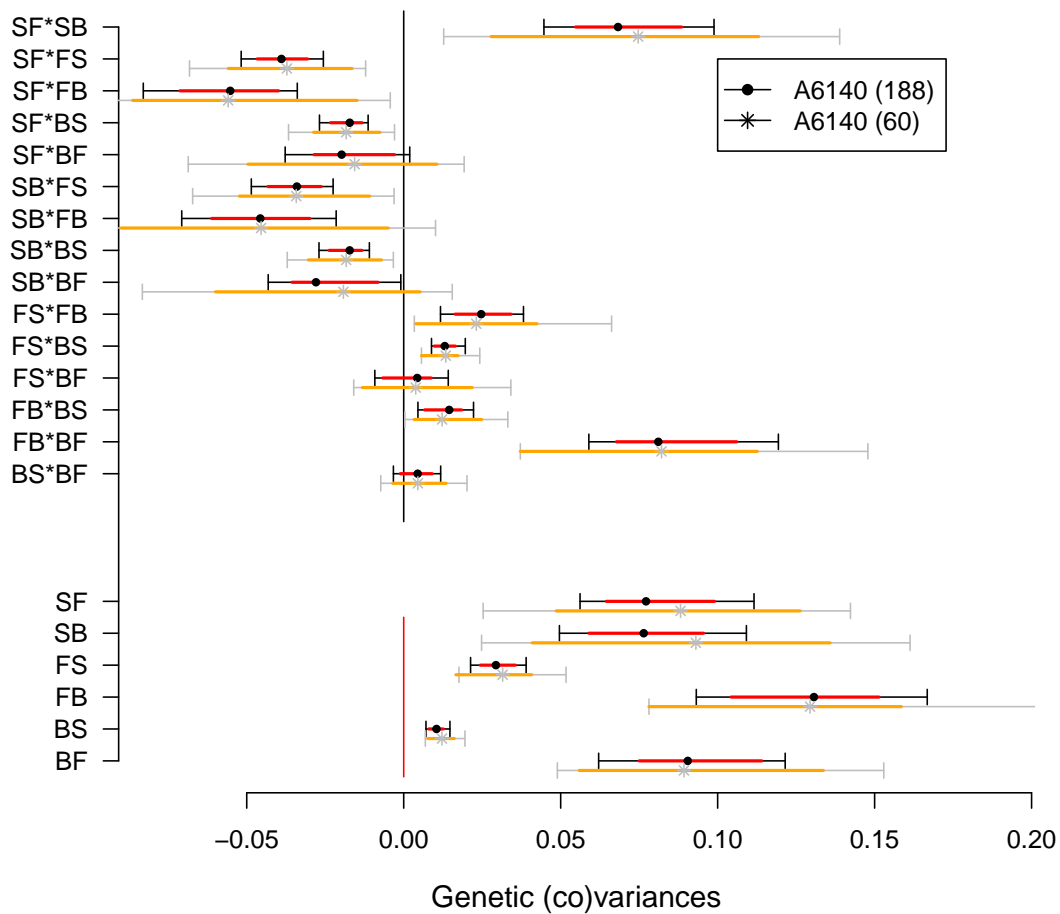


Figure S8: G-matrix estimates of the 140-generation domesticated A6140 population. Black and red show the estimated genetic (co)variances using all inbred lines as in main Figure 3. Grey and orange show genetic (co)variances after downsampling to 60 inbred lines, approximately the minimum number of lines phenotyped in the CA[1-3] populations. Median estimates are similar between data sets, though with larger intervals in the subsampled estimates.

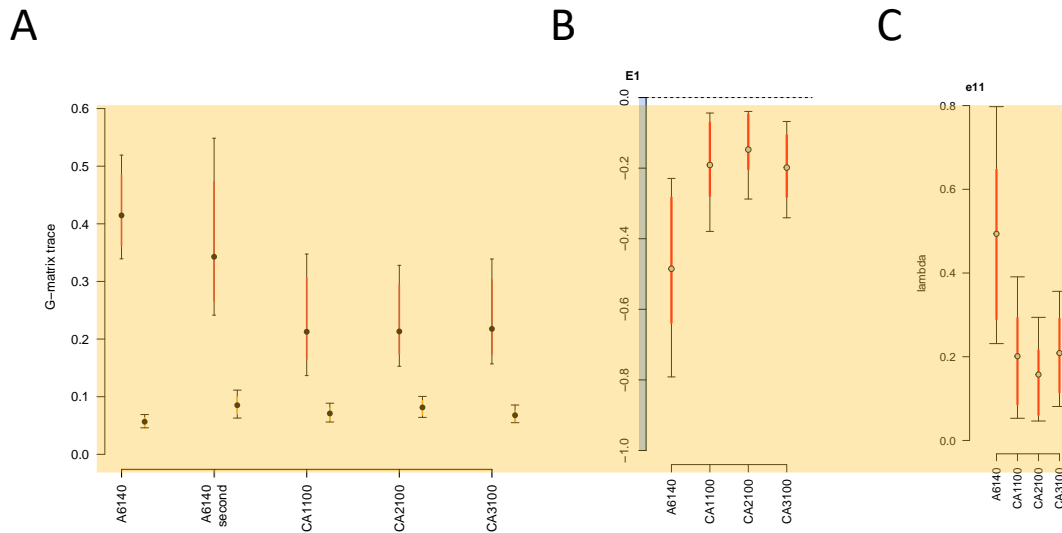


Figure S9: Effect of the common garden assay on genetic (co)variances. **A.** Total amount of genetic variance computed as the sum of the **G**-matrix diagonal elements (trace). The amount of genetic variance in the two A6140 matrices from the two separate common gardens is similar. All observed posterior means differ from the null 95% posterior means (orange). **B.** The coordinates of the **G**-matrices in the space of the first eigentensor when comparing the A6140 and the CA[1-3]100 populations, all computed from the third common garden assay (see Methods). The absolute values of the **G**-matrix coordinates in each eigentensor represent its contribution to the difference between matrices. Coordinates with opposing signs indicate that the matrices contribute in opposing directions. **C.** Contribution of specific trait combinations to coordinated changes among **G**-matrices. Each panel shows the amount of genetic variance in the direction of the greatest variation among **G** (eigenvector of  $E_1$  only). Here, as in panels **A.** and **B.**, the results obtained from this second A6140 **G**-matrix are similar to when using the one from the first common garden assay.

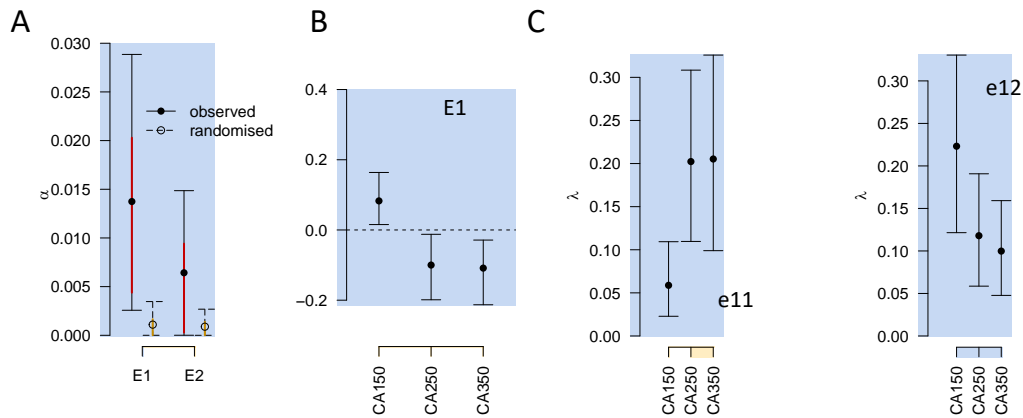


Figure S10: Genetic differentiation. **A.** Eigentensor decomposition of variation among **G**-matrices of the CA[1-3]50 populations. The variance  $\alpha_i$  associated with the  $i$ th eigentensor  $E_i$  is compared to a null permutation model where variation among matrices is due to sampling (see Methods). Here, only the first eigentensors is different from the null. **B.** The coordinates of the **G**-matrices in the space of the first eigentensor. The absolute values of the matrices coordinates in each eigentensor represent its contribution to the difference between matrices. Coordinates with opposing signs indicate that the matrices contribute in opposing directions. **C.** Contribution of specific trait combinations to coordinated changes among **G**-matrices. Each panel shows the amount of genetic variance in the direction of the greatest variation among **G** (eigenvector of  $E_1$  only).



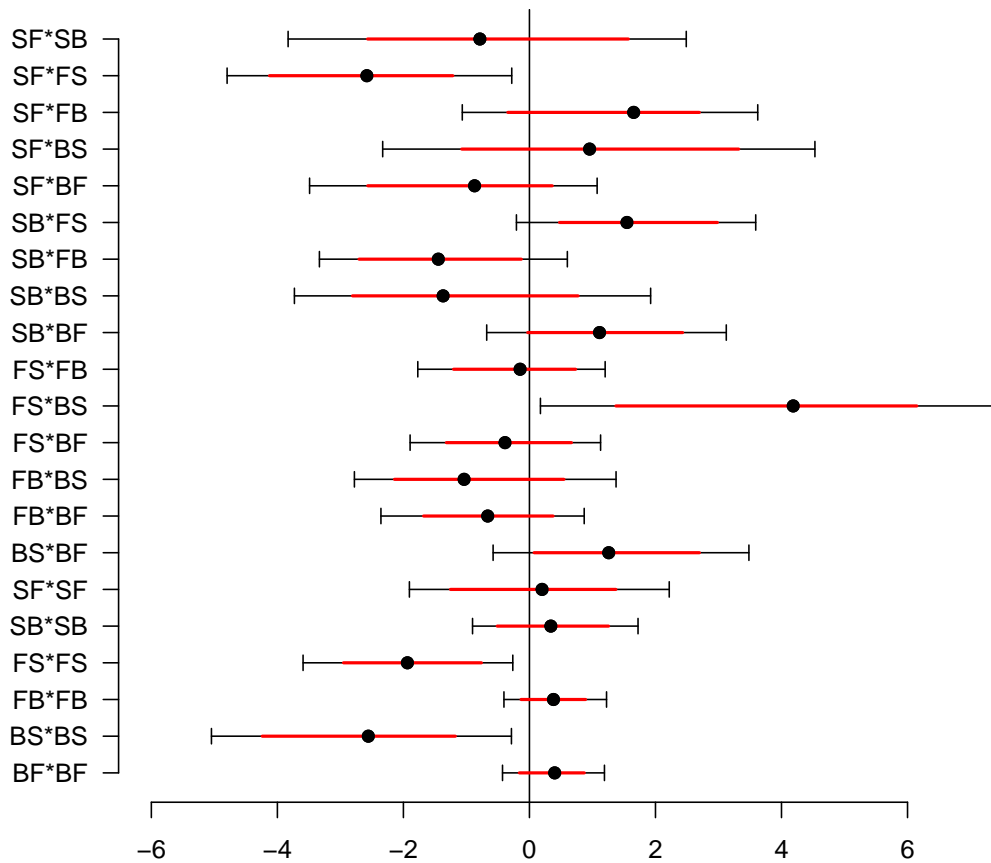


Figure S11: Quadratic selection coefficients. The partial regression coefficients of fertility on transition rates estimated by Bayesian inference. Each row shows the mode (dot), and 83% and 95% credible intervals (red bar and line bars, respectively) of the posterior distributions. The top 15 rows show coefficients of correlated selection between two transition rates, the bottom 6 rows show coefficients of stabilizing or disruptive selection on each transition rate.

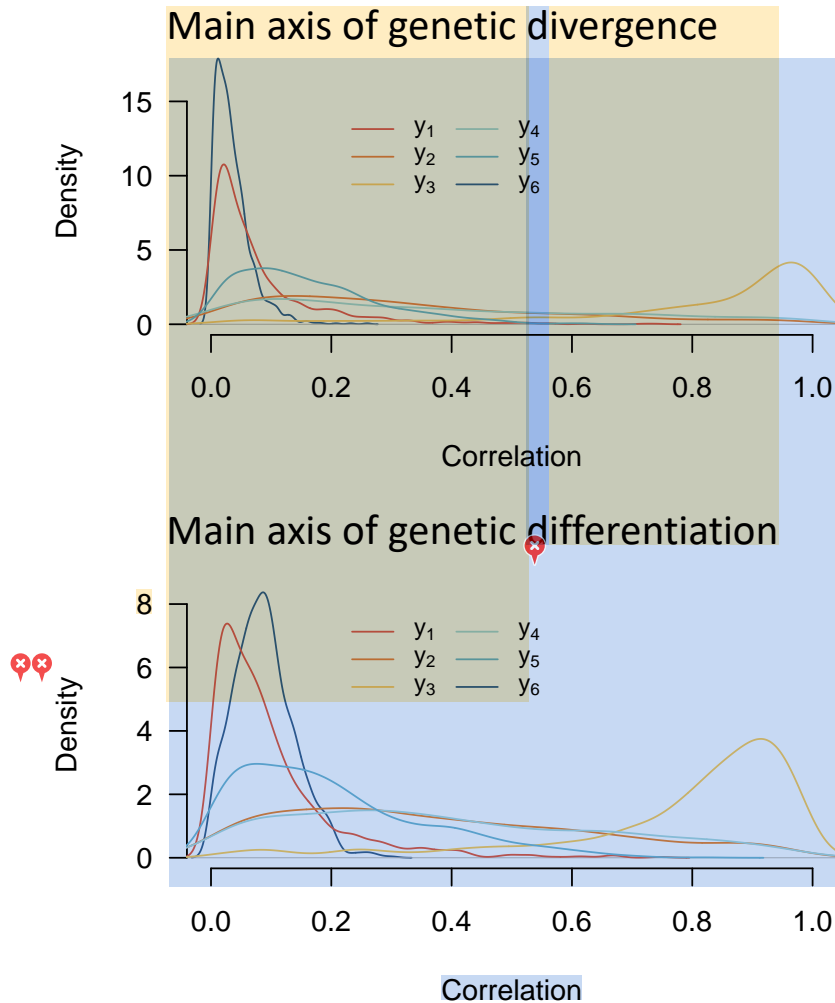


Figure S12: Alignment of  $G$ -matrices divergence and differentiation with the quadratic selection surface. Shown is the density distributions of Pearson product moment correlations between the first eigenvector  $e_{11}$  of  $E1$  measured for divergence (between A6140 and CA[1-3]50, top panel) and for genetic differentiation (measured among CA[1-3]50, bottom panel). The density distributions are obtained from 1000 sampling in the posterior distribution of the  $\gamma$  matrix.

## 11 Tables

Transition rate	Sex	Chisq	P value	P adjusted
SF	H	0.542	0.462	0.799
SB	H	0.715	0.398	0.799
FS	H	0.389	0.533	0.799
FB	H	3.077	0.079	0.799
BS	H	0.037	0.847	0.924
BF	H	1.810	0.179	0.799
SF	M	0.414	0.520	0.799
SB	M	0.647	0.421	0.799
FS	M	0.542	0.462	0.799
FB	M	0.053	0.817	0.924
BS	M	0.001	0.980	0.980
BF	M	0.082	0.774	0.924

Table 1: Phenotypic stasis: Results of anova LRT  $\chi_1^2$  tests for directional changes in mean transition rates in hermaphrodites (H) and males (M), during the 240 generations of lab evolution. Corrected P values for multiple comparisons were obtained with the Benjamini-Hochberg method. Transition rates notation XY stands for transition from trait X to Y, S: Still, F: Forward and B: Backward.

Transition rates	Chisq	P values	P adjusted
SF	5.445	0.020	0.118
SB	1.319	0.251	0.419
FS	0.107	0.743	0.860
FB	1.443	0.230	0.419
BS	1.170	0.279	0.419
BF	0.031	0.860	0.860

Table 2: Inbreeding effects: Results of anova LTR  $\chi_1^2$  testing for mean phenotypic differences between the mean of the inbred lines and the mean of the A6140 population from which they were derived. Corrected P values for multiple comparisons were obtained with the Benjamini-Hochberg method. Transition rates notation XY stands for transition from trait X to Y, S: Still, F: Forward and B: Backward.

	A6140 population					
	$g_{\max}$	$g_2$	$g_3$	$g_4$	$g_5$	$g_6$
Eigenvalues	0.263	0.105	0.022	0.01	0.005	0.003
HPD lower	0.196	0.074	0.016	0.007	0.003	0.002
HPD upper	0.348	0.156	0.03	0.014	0.006	0.003
Proportion	0.645	0.257	0.054	0.025	0.012	0.007
<i>Trait loadings:</i>						
SF	-0.438	0.474	0.086	0.286	-0.539	-0.451
SB	-0.423	0.444	-0.488	0.198	0.501	0.31
FS	0.214	-0.315	-0.176	0.717	0.297	-0.472
FB	0.629	0.383	-0.596	-0.162	-0.236	-0.143
BS	0.112	-0.127	-0.074	0.533	-0.488	0.666
BF	0.419	0.563	0.602	0.234	0.276	0.119

Table 3: Eigendecomposition of the A6140 G-matrix. Transition rates notation XY stands for transition from trait X to Y, S: Still, F: Forward and B: Backward.

	Gamma					
	Y <sub>1</sub>	Y <sub>2</sub>	Y <sub>3</sub>	y <sub>4</sub>	Y <sub>5</sub>	Y <sub>6</sub>
Eigenvalues	4.904	0.256	0.02	-0.172	-1.489	-10.256
HPD lower	0.239	0.008	-0.14	-1.031	-3.456	-18.076
HPD upper	12.295	1.094	0.234	0.036	-0.46	-3.9
Proportion	0.287	0.015	0.001	0.01	0.087	0.6
<i>Trait loadings:</i>						
SF	0.527	-0.429	-0.212	0.378	0.544	-0.234
SB	-0.479	-0.167	-0.744	-0.251	0.3	0.192
FS	-0.296	0.282	0.274	-0.276	0.536	-0.628
FB	0.514	-0.132	0.026	-0.839	0.039	0.112
BS	-0.11	0.016	0.447	0.062	0.548	0.695
BF	-0.359	-0.831	0.356	-0.104	-0.154	-0.135

Table 4: Eigendecomposition of the  $\gamma$  G-matrix. Transition rates notation XY stands for transition from trait X to Y, S: Still, F: Forward and B: Backward.

## 12 Literature Cited

673

674 Aguirre, J. D., Hine, E., McGuigan, K., and Blows, M. W. (2014). Comparing g: multivariate  
675 analysis of genetic variation in multiple populations. *Heredity (Edinb)*, 112(1):21–9.

676 Arnold, S., Pfender, M., and Jones, A. G. (2001). The adaptive landscape as a conceptual bidge  
677 between micro and macroevolution. *Genetica*, 112-113:9–32.


678 Arnold, S. J. (2014). Phenotypic evolution: the ongoing synthesis (american society of naturalists  
679 address). *Am Nat*, 183(6):729–46.


680 Austin, P. C. and Hux, J. E. (2002). A brief note on overlapping confidence intervals. *Journal of*  
681 *vascular surgery*, 36(1):194–195.

682 Baer, C. F., Shaw, F., Steding, C., Baumgartner, M., Hawkins, A., Houppert, A., Mason, N., Reed,  
683 M., Simonelic, K., Woodard, W., and Lynch, M. (2005). Comparative evolutionary genetics  
684 of spontaneous mutations affecting fitness in rhabditid nematodes. *Proc Natl Acad Sci U S A*,  
685 102(16):5785–90.

686 Barr, M. M., García, L. R., and Portman, D. S. (2018). Sexual dimorphism and sex differences in  
687 *caenorhabditis elegans* neuronal development and behavior. *Genetics*, 208(3):909–935.

688 Barton, N. H. (1990). Pleiotropic models of quantitative variation. *Genetics*, 124(3):773–782.

689 Barton, N. H., Etheridge, A. M., and Veber, A. (2017). The infinitesimal model: Definition,  
690  derivation, and implications. *Theor Popul Biol*, 118:50–73.

691  Barton, N. H. and Turelli, M. (1987). Adaptive landscapes, genetic distance and the evolution of  
692 quantitative characters. *Genet Res*, 49(2):157–73.

693 **Bartoń**, K. (2020). *MuMIn: Multi-Model Inference*. R package version 1.43.17.

694 Bernstein, M. R., Zdraljevic, S., Andersen, E. C., and Rockman, M. V. (2019). Tightly linked  
695 antagonistic-effect loci underlie polygenic phenotypic variation in *c. elegans*. *Evol Lett*, 3(5):462–  
696 473.

697 Biquet, J., Bonamour, S., de Villemereuil, P., de Franceschi, C., and Teplitsky, C. (2022). Phenotypic  
698 plasticity drives phenological changes in a mediterranean blue tit population. *J Evol Biol*,  
699 35(2):347–359.

700 Bladt, M. and Sorensen, M. (2005). Statistical inference for discretely observed Markov jump  
701 processes. *Journal of the Royal Statistical Society: Series B (Statistical Methodology)*, 67(3):395–410.

702 Blows, M. W. and Brooks, R. (2003). Measuring nonlinear selection. *Am Nat*, 162(6):815–20.

703 Bohren, B., Hill, W., and Robertson, A. (1966). Some observations on asymmetrical correlated  
704 responses to selection. *Genet Res*, 7:44.

705 Burger, R. (2000). *The Mathematical Theory of Selection, Recombination, and Mutation*. Wiley Series  
706 in Mathematical and Computational Biology. John Wiley Sons, Ltd., New York.

707 Carvalho, S., Chelo, I. M., Goy, C., and Teotónio, H. (2014a). The role of hermaphrodites in the  
708 experimental evolution of increased outcrossing rates in *Caenorhabditis elegans*. *BMC Evol Biol*,  
709 14:116.

710 Carvalho, S., Phillips, P., and Teotónio, H. (2014b). Hermaphrodite life history and the mainte-  
711 nance of partial selfing in experimental populations of *Caenorhabditis elegans*. *BMC Evol Biol*,  
712 14:117.

713 Charlesworth, B., Lande, R., and Slatkin, M. (1982). A neo-darwinian commentary on macroevo-  
714 lution. *Evolution*, 36(3):474–498.

715 Chebib, J. and Guillaume, F. (2017). What affects the predictability of evolutionary constraints us-  
716 ing a g-matrix? the relative effects of modular pleiotropy and mutational correlation. *Evolution*,  
717 71(10):2298–2312.



718 Chelo, I. M., Afonso, B., Carvalho, S., Theologidis, I., Goy, C., Pino-Querido, A., Proulx, S., and  
719 Teotónio, H. (2019). Partial selfing can reduce genetic loads while maintaining diversity during  
720 evolution. *G3 (Bethesda)*, 9:2811–2821.

721 Chelo, I. M., Nédli, J., Gordo, I., and Teotónio, H. (2013). An experimental test on the probability  
722 of extinction of new genetic variants. *Nature Communications*, 4:10.1038/ncomms3417.

723 Chelo, I. M. and Teotónio, H. (2013). The opportunity for balancing selection in experimental  
724 populations of *Caenorhabditis elegans*. *Evolution*, 67(1):142–56.

725 Chen, T. and Guestrin, C. (2016). Xgboost: A scalable tree boosting system. In *Proceedings of the*  
726 *22Nd ACM SIGKDD International Conference on Knowledge Discovery and Data Mining, KDD '16*,  
727 pages 785–794, New York, NY, USA. ACM.

728 Cohan, F. (1984). Can uniform selection retard random genetic divergence between isolated  
729 conspecific populations. *Evolution*, 38:495–504.

730 Cook, D. E., Zdraljevic, S., Roberts, J. P., and Andersen, E. C. (2017). Cendr, the *Caenorhabditis*  
731 *elegans* natural diversity resource. *Nucleic Acids Res*, 45(D1):D650–D657.

732 Czorlich, Y., Aykanat, T., Erkinaro, J., Orell, P., and Primmer, C. R. (2022). Rapid evolution in  
733 salmon life history induced by direct and indirect effects of fishing. *Science*, 376(6591):420–423.

734 de Villemereuil, P., Charmantier, A., Arlt, D., Bize, P., Brekke, P., Brouwer, L., Cockburn, A., Côté,  
735 S. D., Dobson, F. S., Evans, S. R., Festa-Bianchet, M., Gamelon, M., Hamel, S., Hegelbach, J., Jer-  
736 stad, K., Kempnaers, B., Kruuk, L. E. B., Kumpula, J., Kvalnes, T., McAdam, A. G., McFarlane,  
737 S. E., Morrissey, M. B., Pärt, T., Pemberton, J. M., Qvarnström, A., Røstad, O. W., Schroeder,  
738 J., Senar, J. C., Sheldon, B. C., van de Pol, M., Visser, M. E., Wheelwright, N. T., Tufto, J., and  
739 Chevin, L.-M. (2020). Fluctuating optimum and temporally variable selection on breeding date  
740 in birds and mammals. *Proceedings of the National Academy of Sciences*, 117(50):31969–31978.

- 741 Dey, S., Proulx, S., and Teotónio, H. (2016). Adaptation to temporally fluctuating environments  
742 by the evolution of maternal effects. *PLoS Biol*, 14(2):e1002388.
- ✖<sub>43</sub> Doroszuk, A., Wojewodzik, M. W., Gort, G., and Kammenga, J. E. (2008). Rapid divergence  
744 of genetic variance-covariance matrix within a natural population. *The American Naturalist*,  
745 171(3):291–304.✖
- ✖<sub>46</sub> Estes, S. and Arnold, S. (2007). Resolving the paradox of stasis: models with stabilizing selection  
✖<sub>47</sub> explain evolutionary divergence on all timescales. *The American Naturalist*, 169(2):227–244.
- ✖<sub>48</sub> Farhadifar, R., Baer, C. F., Valfort, A. C., Andersen, E. C., Muller-Reichert, T., Delattre, M., and  
749 Needleman, D. J. (2015). Scaling, selection, and evolutionary dynamics of the mitotic spindle.  
750 *Curr Biol*, 16:732–740.
- 751 Flavell, S. W., Raizen, D. M., and You, Y.-J. (2020). Behavioral states. *Genetics*, 216(2):315–332.
- ✖<sub>52</sub> Fowler, K. and Whitlock, M. C. (1999). The distribution of phenotypic variance with inbreeding.  
✖<sub>53</sub> *Evolution*, 53(4):1143–1156.
- 754 Gingerich, P. D. (2019). *Rates of evolution: a quantitative synthesis*. Cambridge University Press.
- 755 Gray, J. M., Hill, J. J., and Bargmann, C. I. (2005). A circuit for navigation in *Caenorhabditis*  
756 *elegans*. *Proc Natl Acad Sci U S A*, 102(9):3184–91.
- 757 Gromko, M. H. (1995). Unpredictability of correlated response to selection: Pleiotropy and sam-  
758 pling interact. *Evolution*, 49(4):685–693.
- 759 Guzella, T., Dey, S., Chelo, I. M., Pino-Querido, A., Pereira, V., Proulx, S., and Teotónio, H. (2018).  
760 Slower environmental change hinders adaptation from standing genetic variation. *PLoS Genet*,  
761 14:e1007731.
- 762 Hadfield, J. (2010). Mcmc methods for multi-response generalized linear mixed models: The  
763 *mcmcglmm* R package. *Journal of Statistical Software*, 33(2):1–22.

- 764 Haller, B. C. and Hendry, A. P. (2014). Solving the paradox of stasis: squashed stabilizing selection  
765 and the limits of detection. *Evolution*, 68(2):483–500.
- 766 Hansen, T. and Martins, E. (1996). Translating between macroevolutionary process and microevo-  
767 lutionary patterns: the correlation structure of interspecific data. *Evolution*, 50:1404–1417.
- 768 Hansen, T. F. and Wagner, G. P. (2001). Modeling genetic architecture: a multilinear theory of  
769 gene interaction. *Theor Popul Biol*, 59(1):61–86.
- 770 Hill, W. G. (1982). Rates of change in quantitative traits from fixation of new mutations. *Proc Natl*  
771 *Acad Sci U S A*, 79(1):142–5.
- 772 Hine, E., Chenoweth, S. F., Rundle, H. D., and Blows, M. W. (2009). Characterizing the evolution  
773 of genetic variance using genetic covariance tensors. *Philosophical Transactions of the Royal Society*  
774 *B: Biological Sciences*, 364(1523):1567–1578.
- 775 Houle, D., Bolstad, G. H., van der Linde, K., and Hansen, T. F. (2017). Mutation predicts 40  
776 million years of fly wing evolution. *Nature*, 548(7668):447–450.
- 777 Houle, D., Morikawa, B., and Lynch, M. (1996). Comparing mutational variabilities. *Genetics*,  
778 143(3):1467–1483.
- 779 Hunt, J., Blows, M. W., Zajitschek, F., Jennions, M. D., and Brooks, R. (2007). Reconciling strong  
780 stabilizing selection with the maintenance of genetic variation in a natural population of black  
781 field crickets (*teleogryllus commodus*). *Genetics*, 177(2):875–880.
- 782 Jackson, C. H. (2011). Multi-state models for panel data: The msm package for R. *Journal of*  
783 *Statistical Software*, 38(8):1–29.
- 784 Johnson, N. A. and Porter, A. H. (2007). Evolution of branched regulatory genetic pathways:  
785 directional selection on pleiotropic loci accelerates developmental system drift. *Genetica*,  
786 129(1):57–70.

787 \* Johnson, T. and Barton, N. (2005). Theoretical models of selection and mutation on quantitative  
788 traits. *Philos Trans R Soc Lond B Biol Sci*, 360(1459):1411–25.

789 Kalbfleisch, J. D. and Lawless, J. F. (1985). The Analysis of Panel Data Under a Markov Assump-  
790 tion. *Journal of the American Statistical Association*, 80(392):863.

791 Kearsey, M. and Pooni, H. (1996). *The Genetical Analysis of Quantitative Traits*. Chapman and Hall,  
792 New York.

793 \* Kruuk, L., Slate, J., Pemberton, J., Brotherstone, S., Guinness, F., and Clutton-Brock, T. (2002).  
794 Antler size in red deer: heritability and selection but no evolution. *Evolution*, 56:1683–1685.

795 Lande, R. (1976). Natural selection and random genetic drift in phenotypic evolution. *Evolution*,  
796 30:314–334.

797 Lande, R. (1979). Quantitative genetic analysis of multivariate evolution, applied to brain: body  
798 size allometry. *Evolution*, 33:402–416.

799 Lande, R. (1980). The genetic covariance between characters maintained by pleiotropic mutations.  
800 *Genetics*, 94(1):203–15.

801 Lande, R. (1986). The dynamics of peak shifts and the pattern of morphological evolution. *Pale-*  
802 *obiology*, 12:343–354.

803 Lande, R. and Arnold, S. J. (1983). On the measurement of selection on correlated characters.  
804 *Evolution*, 37:1210–1226.

805 Lee, D., Zdraljevic, S., Stevens, L., Wang, Y., Tanny, R. E., Crombie, T. A., Cook, D. E., Webster,  
806 A. K., Chirakar, R., Baugh, L. R., et al. (2021). Balancing selection maintains hyper-divergent  
807 haplotypes in *Caenorhabditis elegans*. *Nature ecology & evolution*, 5(6):794–807.

808 Lipton, J., Kleemann, G., Ghosh, R., Lints, R., and Emmons, S. W. (2004). Mate searching  
809 in *Caenorhabditis elegans*: a genetic model for sex drive in a simple invertebrate. *J Neurosci*,  
810 24(34):7427–34.

811 Lynch, M. and Hill, W. G. (1986). Phenotypic evolution by neutral mutation. *Evolution*, 40(5):915–  
812 935.

813 Lynch, M. and Walsh, B. (1998). *Genetics and Analysis of Quantitative Traits*. Sinauer Associates,  
814 Inc., Sunderland.

815 Mallard, F., Afonso, B., and Teotónio, H. (2022a). Selection and the direction of phenotypic  
816 evolution. *bioRxiv*, page 2022.05.28.493855.

817 Mallard, F., Noble, L., Baer, C. F., and Teotónio, H. (2022b). Variation in mutational (co)variances.  
818 *G3 Genes—Genomes—Genetics*.

819 Matuszewski, S., Hermisson, J., and Kopp, M. (2015). Catch me if you can: adaptation from  
820 standing genetic variation to a moving phenotypic optimum. *Genetics*, 200:1255–1274.

821 Merilä, J., Sheldon, B. C., and Kruuk, L. E. (2001). Explaining stasis: microevolutionary studies  
822 in natural populations. *Genetica*, 112-113:199–222.

823 Morrissey, M. B. (2015). Evolutionary quantitative genetics of nonlinear developmental systems.  
824 *Evolution*, 69(8):2050–66.

825 Morrissey, M. B. and Bonnet, T. (2019). Analogues of the fundamental and secondary theorems  
826 of selection, assuming a log-normal distribution of expected fitness. *J Hered*, 110(4):396–402.


827 Morrissey, M. B. and Hadfield, J. D. (2012). Directional selection in temporally replicated studies  
828 is remarkably consistent. *Evolution*, 66(2):435–42.

829 Noble, L. M., Chelo, I., Guzella, T., Afonso, B., Riccardi, D. D., Ammerman, P., Dayarian, A.,  
830 Carvalho, S., Crist, A., Pino-Querido, A., Shraiman, B., Rockman, M. V., and Teotónio, H.  
831 (2017). Polygenicity and epistasis underlie fitness-proximal traits in the *Caenorhabditis elegans*  
832 multiparental experimental evolution (ceme) panel. *Genetics*, 207(4):1663–1685.

833 Noble, L. M., Rockman, M. V., and Teotónio, H. (2019). Gene-level quantitative trait mapping in  
834 *C. elegans*. *G3 Genes—Genomes—Genetics*.

- 835 Phillips, P., Whitlock, M. C., and Fowler, G. R. (2001). Inbreeding changes the shape of the genetic  
836 covariance matrix in *Drosophila melanogaster*. *Genetics*, 158:1137–1145.
- 837 Phillips, P. C. and Arnold, S. J. (1989). Visualizing multivariate selection. *Evolution*, 43(6):1209–  
838 1222.
- 839 Poulet, N., Vielle, A., Gimond, C., Carvalho, S., Teotónio, H., and Braendle, C. (2016). Complex  
840 heterochrony underlies the evolution of *Caenorhabditis elegans* hermaphrodite sex allocation.  
841 *Evolution*, 30:2357–2369.
- 842 Pujol, B., Blanchet, S., Charmantier, A., Danchin, E., Facon, B., Marrot, P., Roux, F., Scotti, I.,  
843 Teplitsky, C., Thomson, C. E., and Winney, I. (2018). The missing response to selection in the  
844 wild. *Trends Ecol Evol*, 33(5):337–346.
- 845 Riska, B. (1989). Composite traits, selection response and evolution. *Evolution*, 43:1172–1191.
- 846 Robertson, A. (1961). Inbreeding in artificial selection programmes. *Genetical Research*, 2(2):189–  
847 194.
- 848 Santiago, E. and Caballero, A. (1998). Effective size and polymorphism of linked neutral loci in  
849 populations under directional selection. *Genetics*, 149(4):2105.
- 850 Schluter, D. (1996). Adaptive radiation along genetic lines of least resistance. *Evolution*,  
851 50(5):1766–1774.
- 852 Scrucca, L., Fop, M., Murphy, T. B., and Raftery, A. E. (2016). mclust 5: clustering, classification  
853 and density estimation using Gaussian finite mixture models. *The R Journal*, 8(1):205–233.
- 854 Shaw, F., Shaw, R. G., Wilkinson, G., and Turelli, M. (1995). Changes in genetic variances and  
855 covariances: G whiz! *Evolution*, 49:1260–1267.
- 856 Simons, Y. B., Bullaughey, K., Hudson, R. R., and Sella, G. (2018). A population genetic interpre-  
857 tation of gwas findings for human quantitative traits. *PLoS Biol*, 16(3):e2002985.

- 858 Simpson, G. G. (1944). *Tempo and Mode in Evolution*. Columbia University Press, New York.
- 859 Simões, P., Fragata, I., Santos, J., Santos, M. A., Santos, M., Rose, M. R., and Matos, M. (2019).  
860 How phenotypic convergence arises in experimental evolution. *Evolution*, 73(9):1839–1849.
- 861 Stan Development Team (2018). RStan: the R interface to Stan. R package version 2.18.2.
- 862 Stiernagle, T. (1999). *Maintenance of C. elegans*. Oxford University Press, Oxford.
- 863 Stinchcombe, J. R., Simonsen, A. K., and Blows, M. W. (2014). Estimating uncertainty in multi-  
864 variate responses to selection. *Evolution*, 68(4):1188–96.
- 865 Swierczek, N. A., Giles, A. C., Rankin, C. H., and Kerr, R. A. (2011). High-throughput behavioral  
866 analysis in *C. elegans*. *Nat Methods*, 8(7):592–8.
- 867 Teotónio, H., Carvalho, S., Manoel, D., Roque, M., and Chelo, I. M. (2012). Evolution of outcross-  
868 ing in experimental populations of *Caenorhabditis elegans*. *PLOS ONE*, 7(4):e35811.
- 869 Teotónio, H., Estes, S., Phillips, P., and Baer, C. (2017). Experimental evolution with caenorhab-  
870 ditis nematodes. *Genetics*, 206(12):691–716.
- 871 Teotónio, H., Manoel, D., and Phillips, P. C. (2006). Genetic variation for outcrossing among  
872 *Caenorhabditis elegans* isolates. *Evolution*, 60(6):1300–1305.
- 873 Teotónio, H., Matos, M., and Rose, M. R. (2004). Quantitative genetics of functional characters in  
874 *Drosophila melanogaster* populations subjected to laboratory selection. *J Genet*, 83:265–277.
- 875 Teotónio, H. and Rose, M. R. (2000). Variation in the reversibility of evolution. *Nature*,  
876 408(6811):463–6.
- 877 Theologidis, I., Chelo, I. M., Goy, C., and Teotónio, H. (2014). Reproductive assurance drives  
878 transitions to self-fertilization in experimental *Caenorhabditis elegans*. *BMC Biology*, 12(1):93.
- 879 Uyeda, J. C., Hansen, T. F., Arnold, S., and Pienaar, J. (2011). The million-year wait for macroevo-  
880 lutionary bursts. *Proceedings of the National Academy of Sciences*, 108:15908–15913.

- 881  Venables, W. and Ripley, B. (2002). *Modern Applied Statistics with S*. Statistics and Computing.  
882 Springer, New York.
- 883 Vladar, H. and Barton, N. (2014). Stability and response of polygenic traits to stabilizing selection  
884 and mutation. *Genetics*, 197:749–767.
- 885 Walter, G. M., Aguirre, J. D., Blows, M. W., and Ortiz-Barrientos, D. (2018). Evolution of genetic  
886 variance during adaptive radiation. *American Naturalist*, 191(4):E108–E128.
- 887 Whitlock, M. C., Phillips, P. C., and Fowler, K. (2002). Persistence of changes in the genetic  
888 covariance matrix after a bottleneck. *Evolution*, 56(10):1968–75.
- 889 Yeh, S.-D., Saxena, A. S., Crombie, T. A., Feistel, D., Johnson, L. M., Lam, I., Lam, J., Saber, S.,  
890 and Baer, C. F. (2017). The mutational decay of male-male and hermaphrodite-hermaphrodite  
891 competitive fitness in the androdioecious nematode *C. elegans*. *Heredity*, 120:1–12.
- 892 Zhang, X. S. and Hill, W. G. (2005). Predictions of patterns of response to artificial selection in  
893 lines derived from natural populations. *Genetics*, 169(1):411–25.